

Petrogenesis and U-Pb and Sm-Nd geochronology of the Taquaral granite: record of an orosirian continental magmatic arc in the region of Corumbá – MS

Petrogênese e Geocronologia (U-Pb e Sm-Nd) do Granito Taquaral: Registro de um Arco Magmático Continental Orosiriano na Região de Corumbá – MS

Letícia Alexandre Redes^{1,2*}, Maria Zélia Aguiar de Sousa^{1,2,3},
Amarildo Salina Ruiz^{1,2,4}, Jean-Michel Lafon^{2,5}

ABSTRACT: The Taquaral Granite is located on southern Amazon Craton in the region of Corumbá, westernmost part of the Brazilian state of Mato Grosso do Sul (MS), near Brazil-Bolivia frontier. This intrusion of batholithic dimensions is partially covered by sedimentary rocks of the Urucum, Tamengo Bocaina and Pantanal formations and Alluvial Deposits. The rock types are classified as quartz-monzodiorites, granodiorites, quartz-monzonites, monzo and syenogranites. There are two groups of enclaves genetically and compositionally different: one corresponds to mafic xenoliths and the second is identified as felsic microgranular enclave. Two deformation phases are observed: one ductile (F_1) and the other brittle (F_2). Geochemical data indicate intermediate to acidic composition for these rocks and a medium to high-K, metaluminous to peraluminous calc-alkaline magmatism, suggesting also their emplacement into magmatic arc settings. SHRIMP zircon U-Pb geochronological data of these granites reveals a crystallization age of 1861 ± 5.3 Ma. Whole rock Sm-Nd analyses provided $\epsilon_{Nd(1.86 Ga)}$ values of -1.48 and -1.28 and T_{DM} model ages of 2.32 and 2.25 Ga, likely indicating a Ryacian crustal source. Here we conclude that Taquaral Granite represents a magmatic episode generated at the end of the Orosirian, as a part of the Amoguija Magmatic Arc.

KEYWORDS: Taquaral Granite; Geochemistry; U-Pb and Sm-Nd Geochronology.

RESUMO: O Granito Taquaral situa-se no sul do Cráton Amazônico, na região de Corumbá, extremo ocidente do estado de Mato Grosso do Sul (MS), próximo à fronteira Brasil-Bolívia. Ocorre como um batólito, sendo parcialmente recoberto pelas rochas sedimentares das formações Urucum, Tamengo, Bocaina e Pantanal e pelas aluviões atuais. Seus litotipos são classificados como quartzo monzodioritos, granodioritos, quartzo-monzonitos, monzogranitos e sienogranitos. Dois tipos de enclaves de natureza e origens diferentes são encontrados, um de composição máfica correspondente a xenólito e outro como enclave microgranular félsico. Observam-se duas fases deformacionais, uma de natureza dúctil (F_1) e outra rúptil (F_2). Os dados geoquímicos indicam composição intermediária a ácida para essas rochas e um magmatismo cálcio-alkalino de médio a alto-K, metaluminoso a peraluminoso e sugerem uma colocação em ambiente de arco. A análise geocronológica pelo método U-Pb (SHRIMP) em zircão foi realizada em um granodiorito aponta para uma idade de $1861 \pm 5,3$ Ma para sua cristalização. Análises Sm-Nd em rocha total fornecem valores de $\epsilon_{Nd(1,86 Ga)}$ de -1,48 e -1,28 e T_{DM} de 2,32 e 2,25 Ga indicando uma provável fonte crustal riaciana. Admite-se que o Granito Taquaral corresponda a um magmatismo desenvolvido no final do Orosiriano, constituinte do Arco Magmático Amoguijá.

PALAVRAS-CHAVE: Granito Taquaral; Geoquímica; Geocronologia U-Pb e Sm-Nd.

¹Post-graduate Program of Geoscience, Exact and Earth Sciences Institute – ICET, Universidade Federal de Mato Grosso – UFMT, Cuiabá (MT), Brazil. E-mail: leticiaredes@hotmail.com

²National Institute of Sciences and Geoscience Technology of the Amazon (Instituto Nacional de Ciência e Tecnologia de Geociências da Amazônia – GEOCIAM), Geosciences Institute of Universidade Federal do Pará – UFPA, Belém (PA), Brazil.

³Department of Mineral Resources, ICET, UFMT, Cuiabá (MT), Brazil. E-mail: prof.mzaguiar@gmail.com

⁴Department of General Geology, ICET, UFMT, Cuiabá (MT), Brazil. E-mail: asruiz@gmail.com

⁵Para-Iso Isotope Geology Laboratory – IG, Universidade Federal do Pará – UFPA, Belém (PA), Brazil. E-mail: lafonjm@ufpa.br

*Corresponding author.

Manuscript ID: 30231. Received: 01/29/2015. Approved: 06/01/2015.

INTRODUCTION

The basement underlying the Neoproterozoic covers in the region of Corumba has been described as part of the Rio Apa Complex (Rio Apa Terrane) which consists of metagranites, orthogneisses, and subordinate amphibolites (Godoi *et al.* 2001).

Several papers have shown the occurrence of Orosirian magmatism over an extensive area in southern Amazon Craton being recognized in the Rio Apa Terrane by Correia Filho *et al.* (1981), Araújo *et al.* (1982), Godoi *et al.* (2001), Lacerda Filho *et al.* (2006), Cordani *et al.* (2010), Brittes *et al.* (2013) and Plens *et al.* (2013). Vargas-Mattos (2010) also describe the occurrence of Orosirian calc-alkaline granitoids in the San Pablo Terrane in Bolivia.

This work aims the understanding of magmatic and deformational evolution of the Taquaral Granite, and consequently of the Orosirian magmatism in the southern Amazon Craton. Therefore, geologic and petrographic characterization were carried out as well as SHRIMP zircon U-Pb dating, geochemistry and Sm-Nd isotopic analyses in order to determine the petrogenesis, time of emplacement, and tectonic setting.

MATERIALS AND METHODS

Twenty four samples were collected from the Taquaral Granite; among them four samples of enclaves and eight samples of diabase dikes.

Macroscopic and microscopic studies were carried out for petrographic characterization. Modal analysis by point-counting was performed on medium- to coarse-grained

samples in which the selective staining technique of feldspars was previously applied according to Hutchinson (1974); while microscopic point-counting was performed on fine-grained samples.

The software Open Stereo was used for structural data analysis (Grohmann *et al.* 2011) and the shear zone rocks were classified according to Sibson (1977).

Geochemical studies were carried out on nine samples of the Taquaral Granite, taking into consideration their spatial distribution and mineralogical and grain size diversity. Samples were prepared and then sent to the Acme Analytical Laboratories (AcmeLab) in Vancouver, Canada, for major, minor and trace elements analyses (Tab. 1) by Inductively Coupled Plasma Emission Spectrometry (ICP-ES) and Inductively Coupled Plasma Mass Spectrometry (ICP-MS).

The procedure for (SHRIMP) zircon U-Pb geochronology of sample RM-07 followed the steps of sieving into 250, 210, 177, 125, 90 and 63 μm size fractions, and separation by magnetic susceptibility and density. A total of 150 zircon crystals were then hand-picked from the 177 – 125 μm size fraction, under a binocular microscope, among which the crystals for analysis were selected. Cathodoluminescence imaging (SEM-CL) and U-Pb geochronology were carried out at the Center for Geochronological Research of the University of Sao Paulo (CPGeo-IGC/USP). The analytical procedures for U-Pb zircon dating by SHRIMP II (Sensitive High Resolution Ion Microprobe) are described in details by Stern (1998), Williams (1998) and Sato *et al.* (2008). Age calculations were performed using the software ISOPLOT/EX (Ludwig 2001)

Sm-Nd whole rock analyses were performed on two samples (RM-07 and RM-09A) at the Isotope Geology Laboratory of the Federal University of Para (Para-Iso),

Table 1. Geochronological data available for the granitic rocks from Alumiador Intrusive Suite obtained by SHRIMP U-Pb on zircon, Rb-Sr, Sm-Nd, Ar-Ar and K-Ar.

Lithostratigraphic Units	References	U-Pb	Rb-Sr		Sm-Nd		Ar-Ar	K-Ar
		Age (Ma)	Age (Ma)	($\text{Sr}^{87}/\text{Sr}^{86}$) _t	T _{DM} (Ga)	$\epsilon\text{Nd}_{(t)}$	Age (Ma)	Age (Ma)
Alumiador Intrusive Suite	Araújo <i>et al.</i> (1982)		1600 ± 40	0.707				
	Cordani <i>et al.</i> (2005)						1060 1300	
	Lacerda Filho <i>et al.</i> (2006)	1867			2.17	-0.68		
	Cordani <i>et al.</i> (2010)	1839 ± 33	1674 ± 17		2.38 2.49	-2.86 -4.20	1302 ± 3 1296 ± 2	1314 ± 9

according to the analytical procedure described by Oliveira *et al.* (2008) and Barreto *et al.* (2014). Approximately 100 mg of pulverized sample were dissolved into Teflon[®] bombs by adding HNO₃, HCl e HF and placing them into a microwave oven. A ¹⁴⁹Sm/¹⁵⁰Nd tracer was previously introduced in order to determine the concentrations of Sm and Nd by isotope dilution. Chemical separation was made by ion-exchange chromatography divided into two stages with resins Biorad DOWEX[™] AG50x8 and Ln Eichrom[®]. Isotopic analyses were carried out using inductively plasma mass spectrometry (ICP-MS), ThermoFinnigan Neptune. Nd-isotopic ratios were corrected for mass fractionation by normalizing to ¹⁴⁶Nd/¹⁴⁴Nd = 0.7219. The decay constant used was 6.54 x 10⁻¹² year⁻¹ (Lugmair & Marti 1978). Model ages were calculated according to the depleted mantle curve through time by De Paolo (1981).

REGIONAL GEOLOGIC SETTING

The Amazon Craton represents one of the main Precambrian geotectonic entities located on the northern part of South America platform. It consists of two shields divided by the Amazon Basin: The Central Brazilian Shield and the Guyana Shield. This work adopted the proposal of Ruiz (2005), who considers the Rio Apa Province as a part of the compartmentation suggested by Tassinari and Macambira (2004) and revised by Cordani *et al.* (2009), in which the Amazon Craton is divided into geochronological provinces formed by successive accretion of juvenile crust to Proterozoic mobile belts (Provinces Maroni-Itacáunas – 2.20 to 1.95 Ga; Ventuari-Tapajós – 1.95 to 1.80 Ga, Rio Negro-Juruena – 1.80 to 1.55 Ga, Rondonian-San Ignacio – 1.50 to 1.30 Ga and Sunsas-Aguapei – 1.15 to 0.90 Ga) surrounding an Archean proto-craton (Central Amazon Province – > 2.3 Ga).

There are two proposals for the geotectonic settings of Rio Apa Terrane. The first one describes this Terrane as an allochthonous crustal fragment geographically separated from the Amazon Craton by the Tucavaca Belt (Barros *et al.* 1982, Del'Arco *et al.* 1982, Litherland *et al.* 1986, Alvarenga & Saes 1992, Brito Neves *et al.* 1995, Trompette *et al.* 1998, Tassinari & Macambira 1999, 2004, Santos *et al.* 2000, 2008, Teixeira *et al.* 2010, Bettencourt *et al.* 2010). The second proposal, by Ruiz *et al.* (2005), Lacerda Filho *et al.* (2006) and Cordani *et al.* (2010), takes into consideration the previous proposal of Almeida (1967) and Amaral (1974), in which the Rio Apa Terrane is described as a prolongation of the Amazon Craton and the basement of Neoproterozoic mobile belts. This work adopted the second proposal thus

considering the Rio Apa Terrane as a southern portion of the Amazon Craton (Fig. 1)

Based on geological and geochronological data, Lacerda Filho *et al.* (2006) indicate that rocks from Rio Apa Province were formed between 1.95 and 1.75 Ga, which are further divided into three geotectonic compartments: Remnant Oceanic Crust (2.2 to 1.95 Ga), Rio Apa Magmatic Arc (1.95 to 1.87 Ga) and Amoguija Magmatic Arc (1.87 to 1.75 Ga). In addition to the units described and chronologically stacked in this work, these authors also describe the Mafic Continental Magmatism (1.79 to 1.78 Ga) and the Rio Perdido Mafic Dike Swarms (914 ± 9 Ma).

The Amoguija Magmatic Arc is comprised by the Alumiador Intrusive Suite and the Serra da Bocaina Formation. The term Alumiador Intrusive Suite, according to Lacerda Filho *et al.* (2006), Godoy *et al.* (2010) and Manzano *et al.* (2012), corresponds to a N-S trending elongated batholith of syeno to monzogranitic composition consisting of gray to pink leucocratic rocks, isotropic to anisotropic. Plens *et al.* (2013) and Nogueira *et al.* (2013) grouped the granitic intrusions of the Amoguija Magmatic Arc into the Alumiador Intrusive Suite.

Lacerda Filho *et al.* (2006) obtained a SHRIMP U-Pb zircon crystallization age of 1,867 Ma from a porphyritic monzogranite and Sm-Nd isotopic data revealed a T_{DM} model age of 2.17 Ga and ε_{Nd} around -0.68, indicating a juvenile arc with some crustal contamination generated in continental margin settings. Cordani *et al.* (2010) presented Ar-Ar and K-Ar data around 1,300 Ma for the volcanic rocks from Serra da Bocaina and plutonic rocks from Alumiador Intrusive Suite. These authors presented a U-Pb zircon age of 1,839 ± 33 Ma and Nd T_{DM} model ages between 2.54 and 2.49 Ga. Table 1 summarizes the geochronological data available for the Alumiador Intrusive Suite.

The San Pablo Terrane (Fig. 2) in Bolivia was first called Crystal Block by Litherland and Klink (1982) and posteriorly called San Pablo by Saes and Leite (1993), Saes and Fragoso Cesar (1994, 1996) and Saes (1999). According to Saes (1999), the lack of Sunsas Group records in the Terrane would justify its individualization. The San Pablo Terrane is bordered by a tectonic discontinuity represented by the San Diablo Front (Litherland *et al.* 1986) or San Diablo Straightening Zone (Pitfield *et al.* 1979, *in* Saes 1999)

For the Correrca Granite, Vargas-Mattos (2010) obtained Pb-Pb zircon ages between 1,920 and 1,895 Ma, and Sm-Nd T_{DM} model ages between 2.8 and 2.9 Ga and ε_{Nd(t)} values of -8.5 and -9.4, which indicates a Paleoproterozoic felsic magmatism in the San Pablo Terrane. These results corroborate the existence of a crustal block on south of the Paragua Terrane, bordered by the San Diablo Shear Zone, as previously proposed by Litherland and Klink (1982) and posteriorly

by Saes and Leite (1993). The Correrca Granite is located in the region of Rincon Del Tigre and Santo Corazon. It is a batholith overlain by sedimentary rocks of the Sunsas Group to the north, by the Boqui Group to the west, and by the Murcielago Group to the south. To the east, it is in fault contact with the Santo Corazon Granitoid Complex.

FIELD AND PETROGRAPHIC ASPECTS

The Taquaral Granite crops out as large and small blocks, massive or weakly foliated and, sometimes, as mylonitic truncated by cataclastic bands, aplite and diabase dikes and pegmatitic pockets. It also occurs as felsic microgranular enclaves

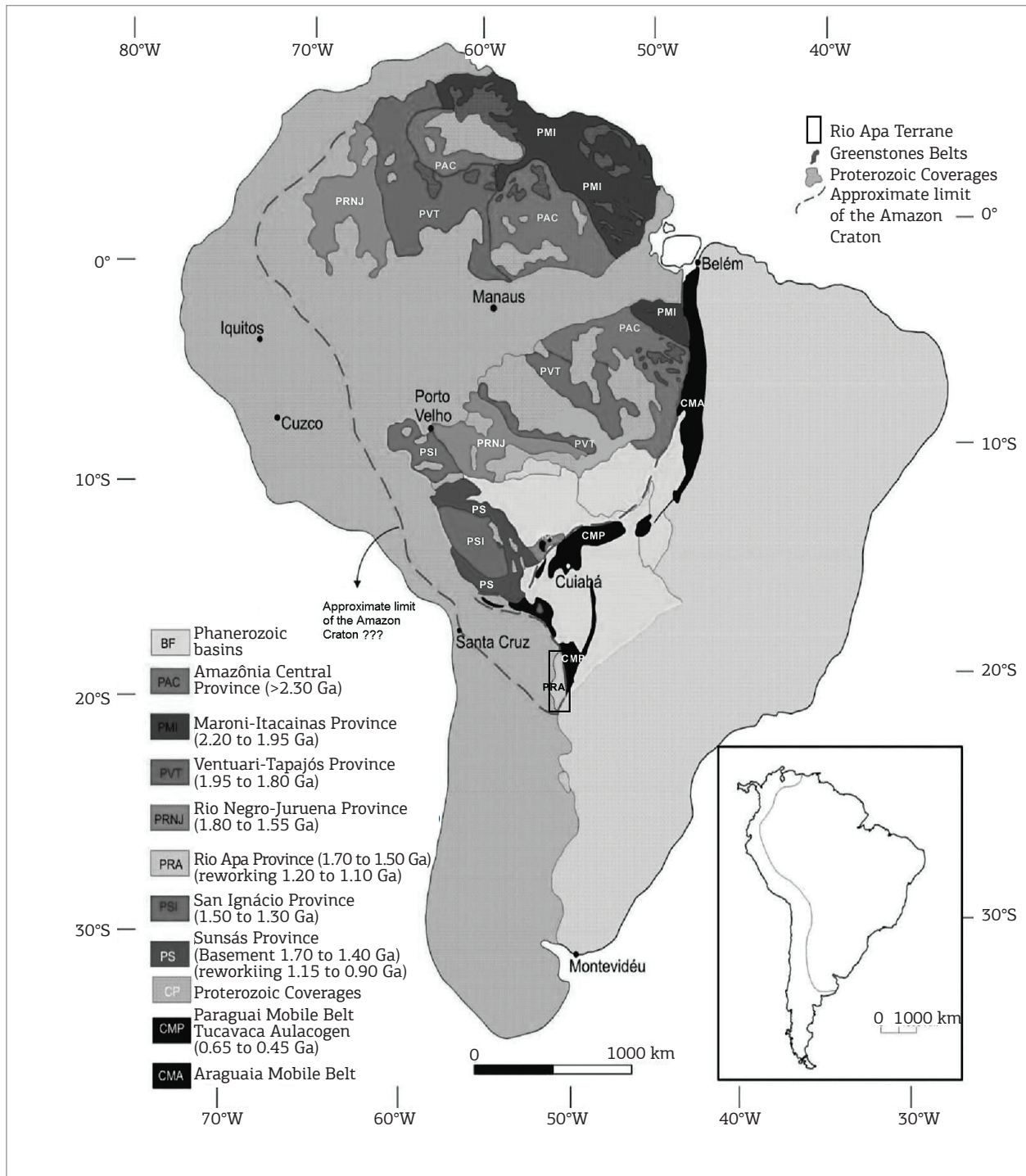


Figure 1. Geochronological and Tectonic Provinces of the Amazon Craton (Ruiz 2005).

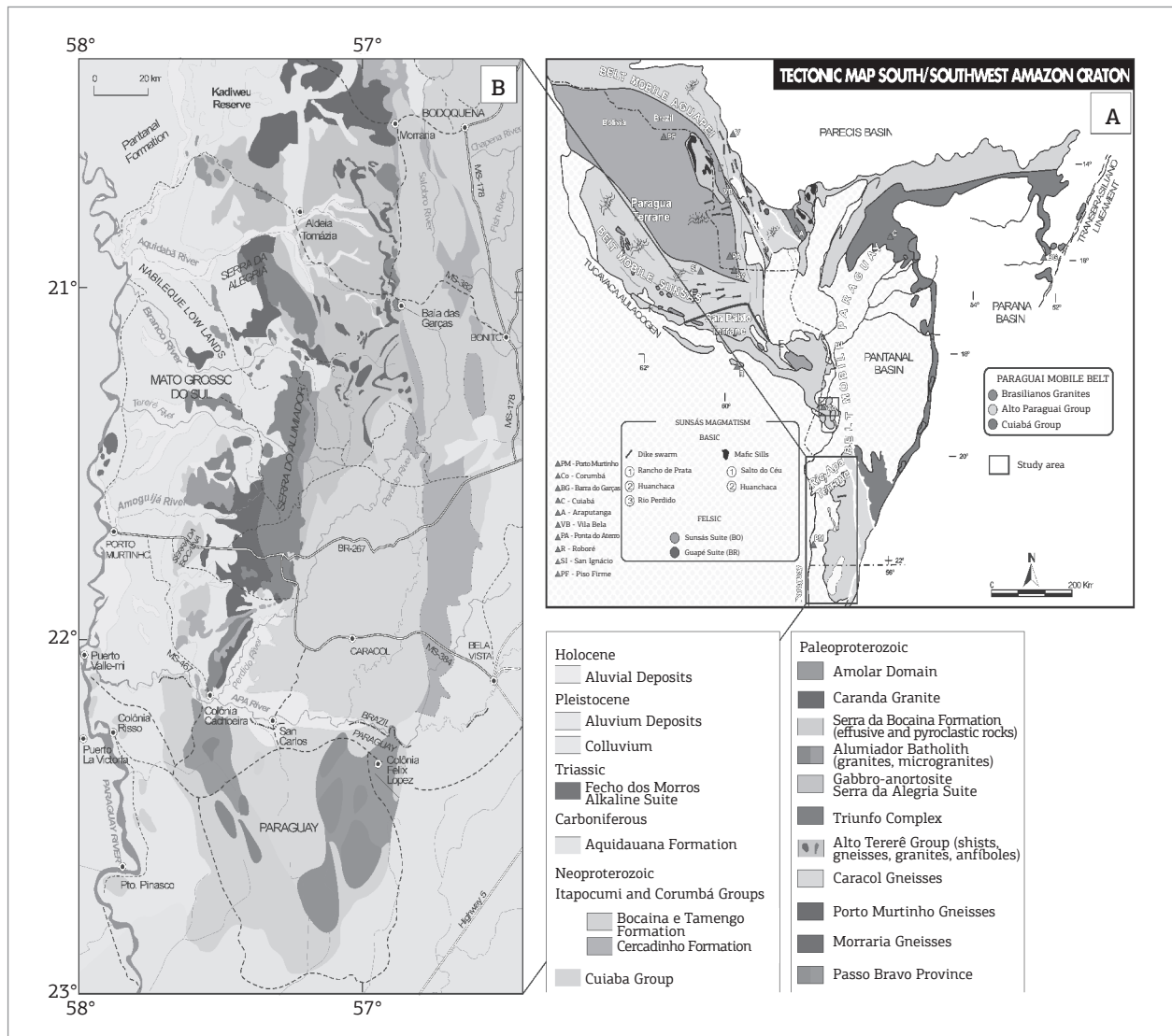
and xenoliths of quartz-diorite and amphibolite, respectively, which are rounded to ellipsoidal, centimetric to decametric. This unit is partially and tectonically overlain by sediments of the Urucum, Tamengo, Bocaina and Pantanal formations and by aluvionar deposits. The contact with the Urucum Formation is only tectonic but the Tamengo and Bocaina formations also partially overlain the granite unconformably.

The study of the Taquaral Granite and detailed geological mapping at a scale of 1:50.000 (Fig. 3) allowed recognize three petrographic facies where it is observed in the field that one facies encompasses another and these are then not discriminated at the mapped scale. The first facies is gray, medium- to coarse-grained (GMCF); the second facies is pink, coarse-grained (PCF) and the third facies is pink, fine-grained (PFF), all of which are massive or weakly foliated containing biotite and amphibole as the major mafic minerals.

Macroscopically, these facies are classified as hornblende-biotite-granitoids and plotted in QAP diagram (Streckeisen 1976; Fig. 4) as quartz-monzodiorites, granodiorites, quartz-monzonites, monzo and syenogranites.

The GMCF predominates volumetrically in the mapped body and is characterized by gray, inequigranular to equigranular medium- to coarse-grained leucocratic rocks, which are classified as quartz-monzodiorite, granodiorite and monzogranite (Figs. 4, 5A and 5B). Pegmatite pockets up to 4 m thick are observed. In the mylonitic portion of this facies, stretched and rotated alkali feldspar porphyroclasts occur in a fine- to medium-grained quartz-feldspathic groundmass which is classified as mylonite (Sibson 1977), based on the relationship between porphyroclasts and groundmass.

The PCF is composed of pink, inequigranular coarse-grained leucocratic rocks, which are classified as quartz-monzonite



and monzogranite (Fig. 4). This facies is distinguished from the others due to the presence of dark-pink subhedral crystals of alkali feldspar up to 3 cm in length (Figs. 5C and 5D).

The PPF consists of light-pink, equi- to inequigranular hololeucocratic rocks of monzo to syenogranite composition (Fig. 4). Aplite dikes occur predominantly as fine-grained rocks, up to 15 cm in thickness, in abrupt and reactive contacts with GMCF and PCF (Figs. 5E and 5F).

Optically, rocks from the GMCF show hipidiomorphic to xenomorphic textures as well as inequigranular to locally graphic textures composed of plagioclase, quartz, alkali feldspar (microcline) and mafic minerals, which are identified as biotite, hornblende, and opaques. Accessory minerals are represented by titanite, apatite, allanite, opaques and zircon (Fig. 6). The mylonites have a fine- to medium-grained groundmass showing porphyroblastic to granoblastic textures. Felsic and mafic minerals are oriented, however they also occur surrounding alkali feldspar porphyroclasts. Quartz aggregates and recrystallized feldspar may occur bordering porphyroclasts and characterizing pressure shadow. This facies is strongly affected by sericitization, argillitization, saussuritization of feldspars, and chloritization of biotite and amphibole as a result of hydrothermal alteration.

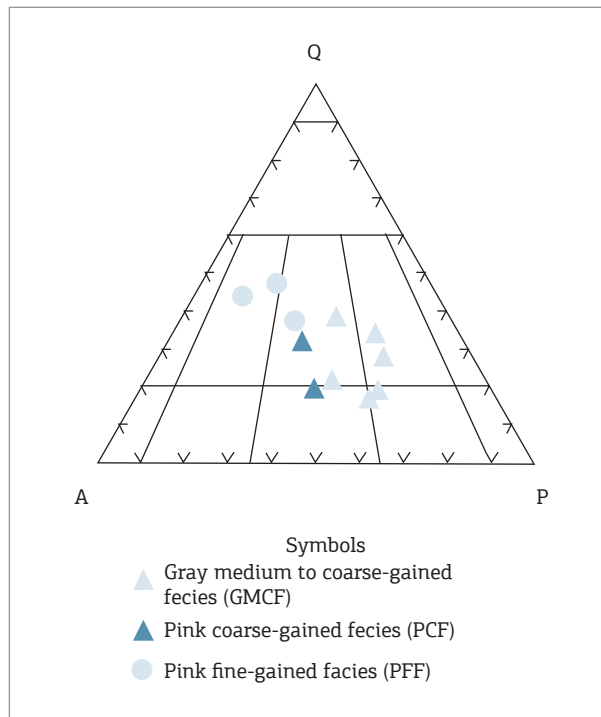


Figure 4. QAP diagram for the rocks from the Taquaral Granite (rock fields according to Le Maitre *et al.* 2002).

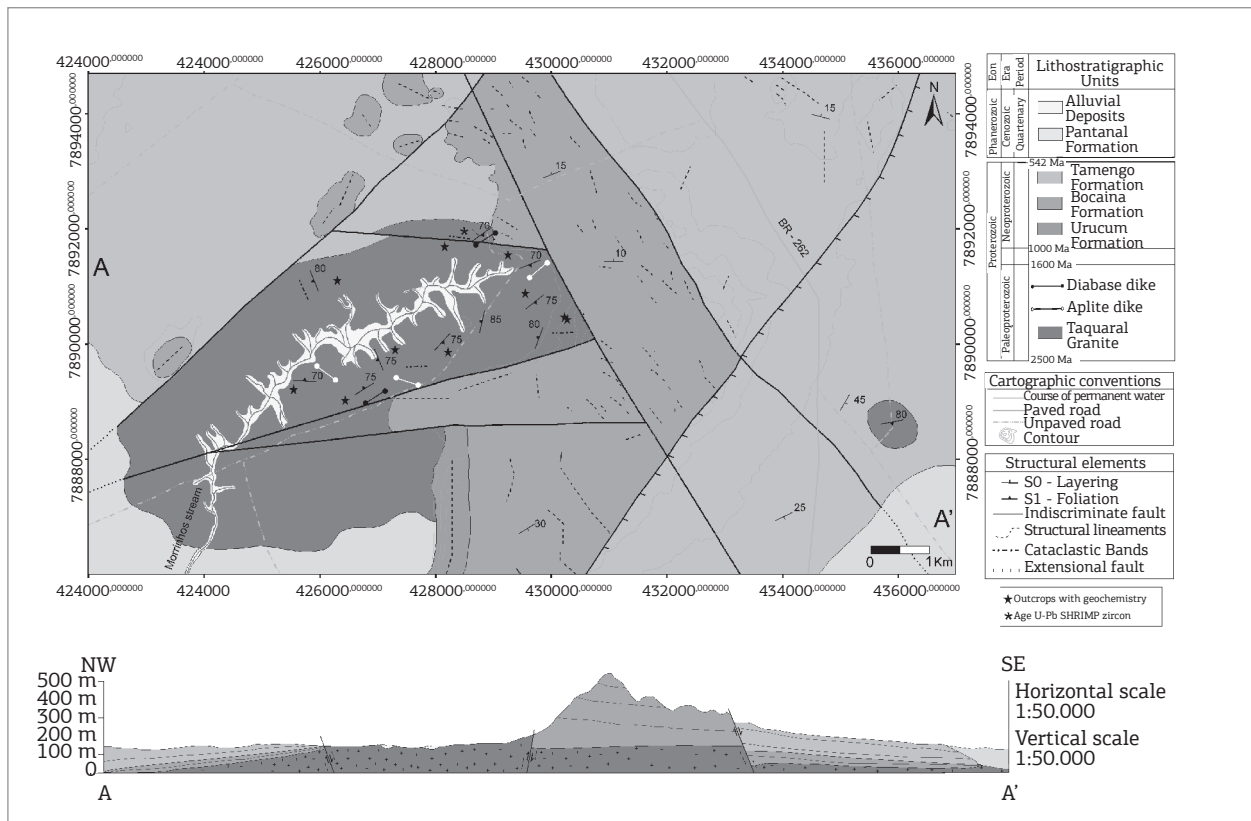


Figure 3. Geological Map of the Taquaral Granite and the Neoproterozoic and Quaternary sedimentary covers.

Microscopically, rocks from the PCF usually displays hipidiomorphic to xenomorphic textures, and rarely graphic texture, consisting of alkali feldspar (perthitic microcline),

plagioclase, quartz, biotite, and amphibole (hornblende) and having titanite, apatite, zircon, opaques as accessory minerals (Fig. 7). The rocks are strongly altered showing

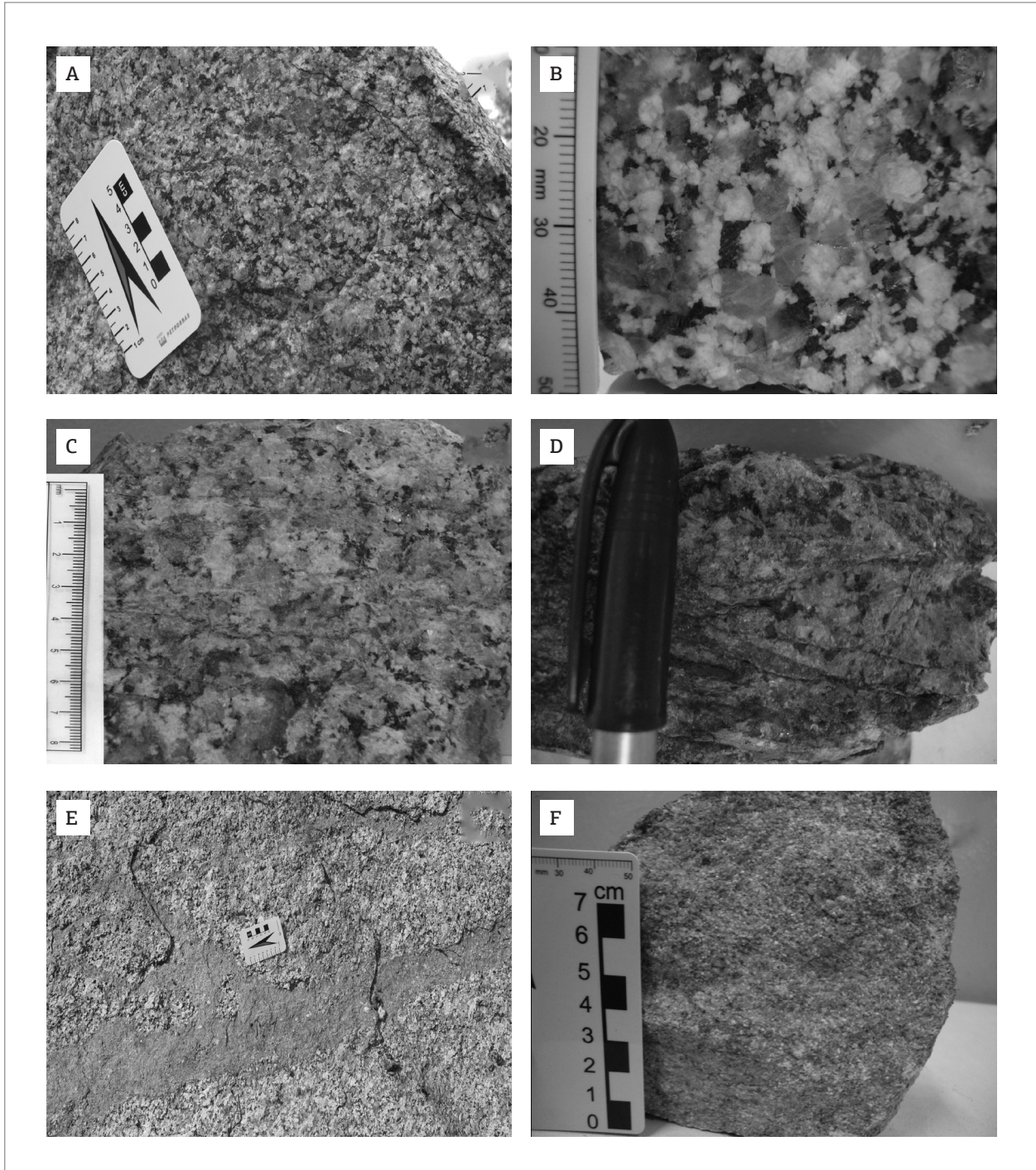


Figure 5. Macroscopic aspects of the Taquaral Granite: (A) medium-grained, weakly foliated, granodiorite from the gray, medium- to coarse-grained facies; (B) gray, inequigranular medium- to coarse-grained granodiorite from the gray, medium- to coarse-grained facies; (C) coarse-grained, well foliated monzogranite from the pink, coarse-grained facies; (D) reddish-pink inequigranular rock displaying cataclastic bands from the pink, coarse-grained facies; (E) aplite dikes pink in color, up to 15 cm thick, in abrupt and reactive contacts with monzogranite, and inclusions of angular fragments from the monzogranitic host; (F) fine-grained aplite of syenogranitic composition from the pink, fine-grained facies.

sericitized or saussuritized feldspars with dusty aspect, as well as chloritized biotite and amphibole.

Under the microscope, rocks from the PPF are predominantly equigranular having xenomorphic texture and consisting of alkali feldspar (microcline), quartz, plagioclase and less than 5% mafic minerals (biotite, hornblende, titanite, apatite and opaques; Figs. 8A and 8B). It is weakly altered with products such as sericite, clay minerals, chlorite and epidote-group minerals, which may occur within micro-veins.

Two enclaves of distinct nature and origin were found in the Taquaral Granite. One of mafic composition corresponds to a xenolith and another is identified as microgranular felsic enclave (MFE) which represents the process of magma mingling (heterogeneous mixing). The xenoliths occurs volumetrically subordinate with amphibolitic composition, elongated, oval to rounded, ranging from centimeter to meter in size, and consisting

of amphibole, plagioclase, opaque minerals and titanite. The centimeter-size MFE is rounded and consists of plagioclase, quartz, alkali feldspars and biotite. Typical features of magma mixing are observed in the MFE at macroscopic and microscopic scales, such as: reactive contact with the host rock, engulfment of xenocrystals, corroded quartz, poikilitic quartz engulfing biotite, hornblende, apatite, and opaque minerals and glomeroporphyros of plagioclase and biotite.

The centimeter- to meter-size dikes truncate the Taquaral Granite in abrupt contacts (Figs. 9A and 9B) and correspond to gabbroic rocks, which were classified as diabase based on grain size and occurrence. Macroscopically, these are massive, dark-gray to black, inequigranular very fine to fine-grained melanocratic rocks composed of variable proportions of plagioclase and mafic minerals (pyroxene, biotite and amphibole; Figs. 9C and 9D).

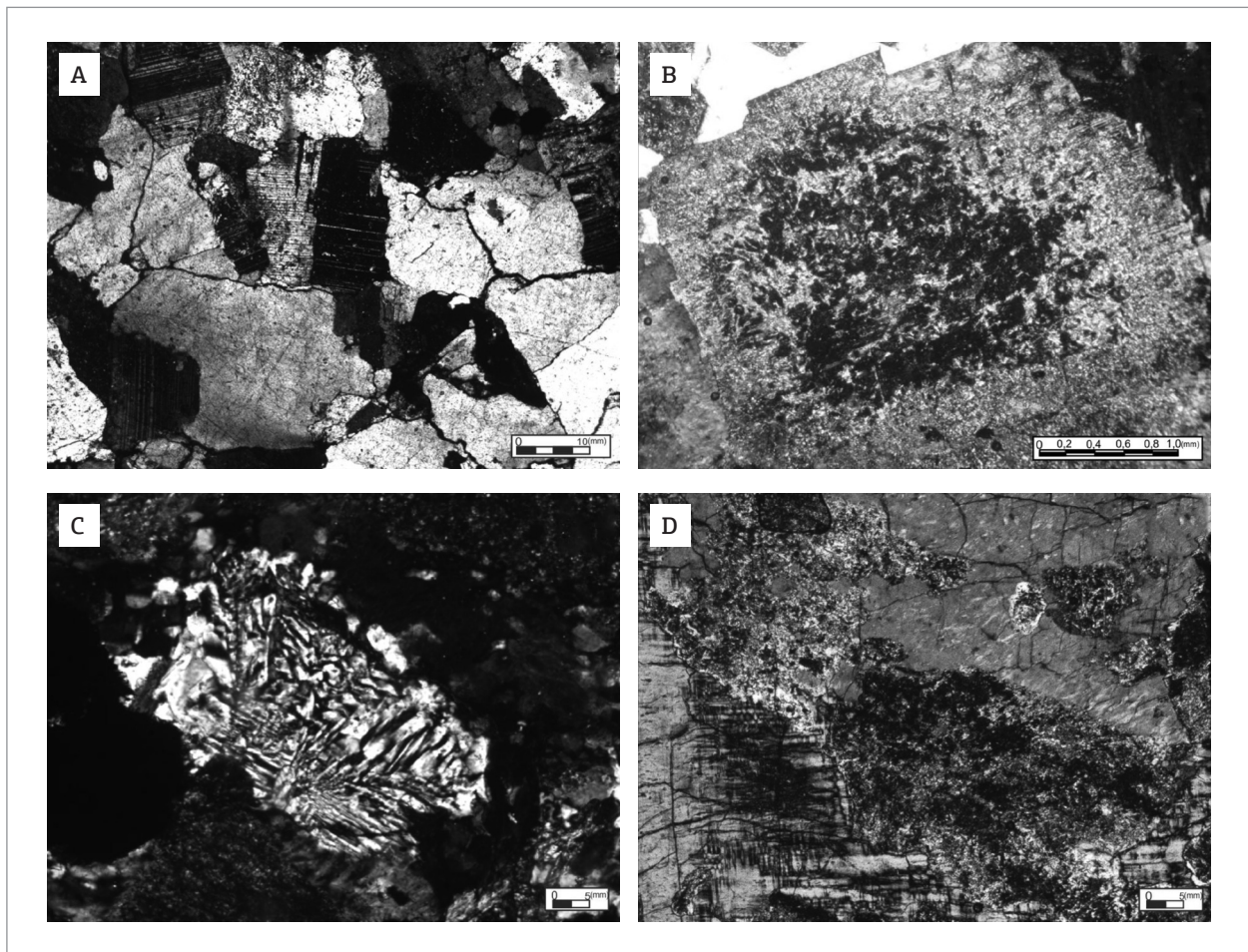


Figure 6. Microphotographs of gray, medium- to coarse-grained facies illustrating: (A) coarse-grained inequigranular texture; (B) plagioclase displaying intensely saussuritized core highlighting normal zoning, being epidote and calcite the main alteration products; (C) Quartz and alkali-feldspar in micrographic texture; (D) perthitic alkali-feldspar in contact with saussuritized plagioclase. Crossed polarizers.

STRUCTURAL ANALYSIS

In order to understand the structural evolution and the kinematics of deformation, which affected the Taquaral Granite, structural analysis was carried out in the study area (Fig. 3). The structural analysis follows the concept of deformation phases according to Sá and Hackspacher (1982) while description and tectonic structures classification, such as foliations and lineations, are according to Passchier and Trouw (2005). Descriptive analysis of field-scale structures associated with examining satellite images and microscopic description allowed the identification of two deformation stages, here called F_1 and F_2 .

Taquaral Granite does not display intense penetrative deformation and rocks are usually isotropic to weakly

foliated. Mylonitic foliation is developed in ductile deformation zones, and cataclasites are widely observed in fault zones. The latter also affected the sedimentary covers of the Corumbá and Jacadigo Groups.

The first deformation phase (F_1) is responsible for the development of incipient penetrative foliation (S_1) being heterogeneous in intensity and orientation (Fig. 10A). A mylonitic banding is observed with development of protomylonites to mylonites indicating strong ductile deformation associated with phase F_1 . Mylonitic foliation is parallel to the regional penetrative foliation (S_1), both of them preferentially oriented to N20-30E, dipping 75°-85° towards the NW.

The rotated plagioclase porphyroclasts occur in a fine- to medium-grained groundmass forming a characteristic

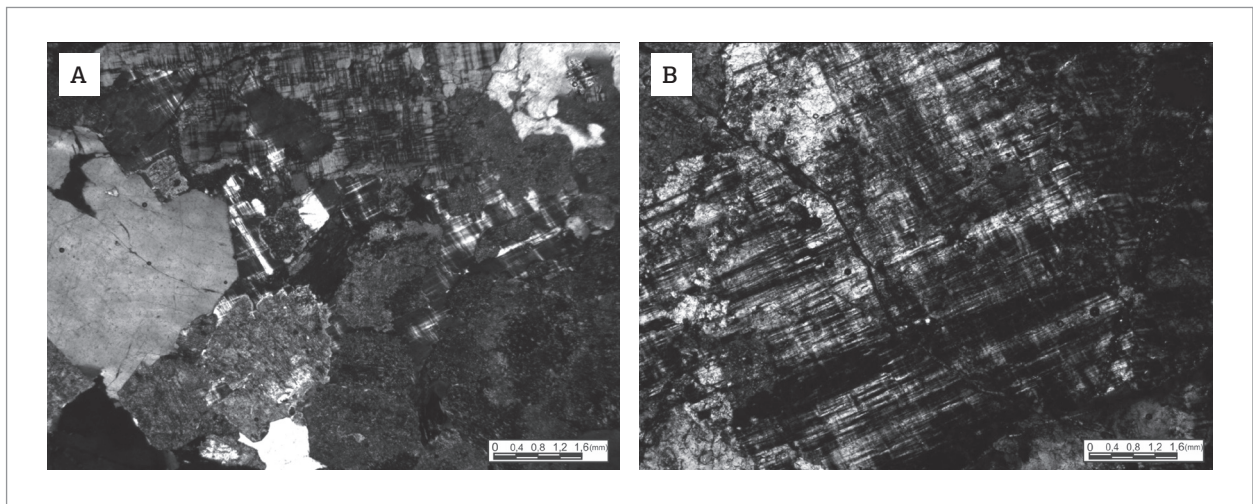


Figure 7. Microphotographs of pink, coarse-grained facies illustrating: (A) coarse-grained equigranular texture; (B) microcline crystal of 8 mm in diameter. Crossed polarizers.

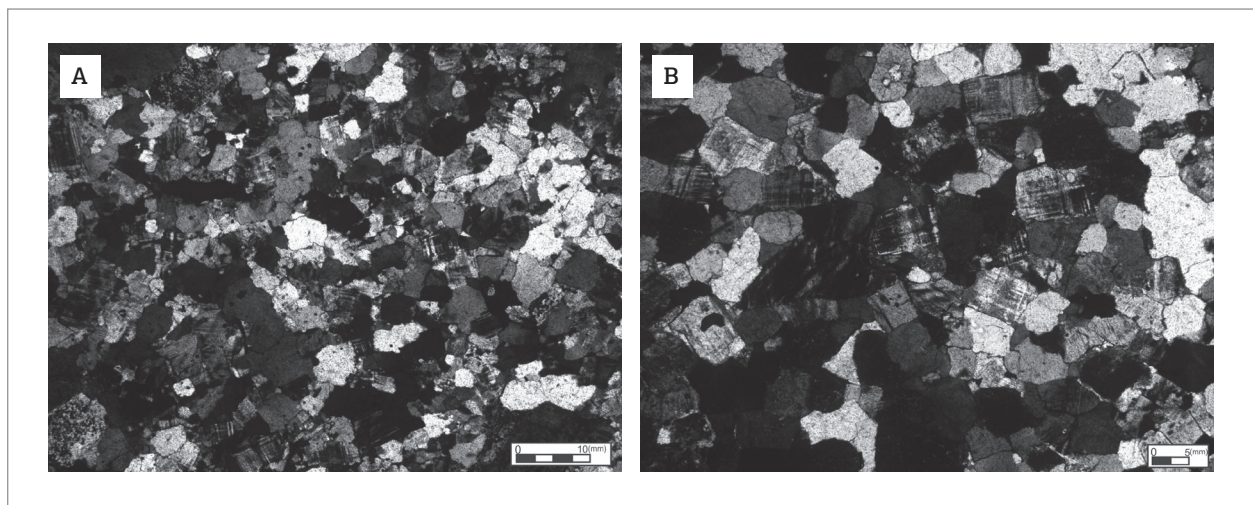


Figure 8. Microphotographs of pink, fine-grained facies: (A) general aspect displaying predominant equigranular xenomorphic texture and saussuritized plagioclase; (B) Xenomorphic texture in detail consisting of quartz, microcline, and saussuritized plagioclase. Crossed polarizers.

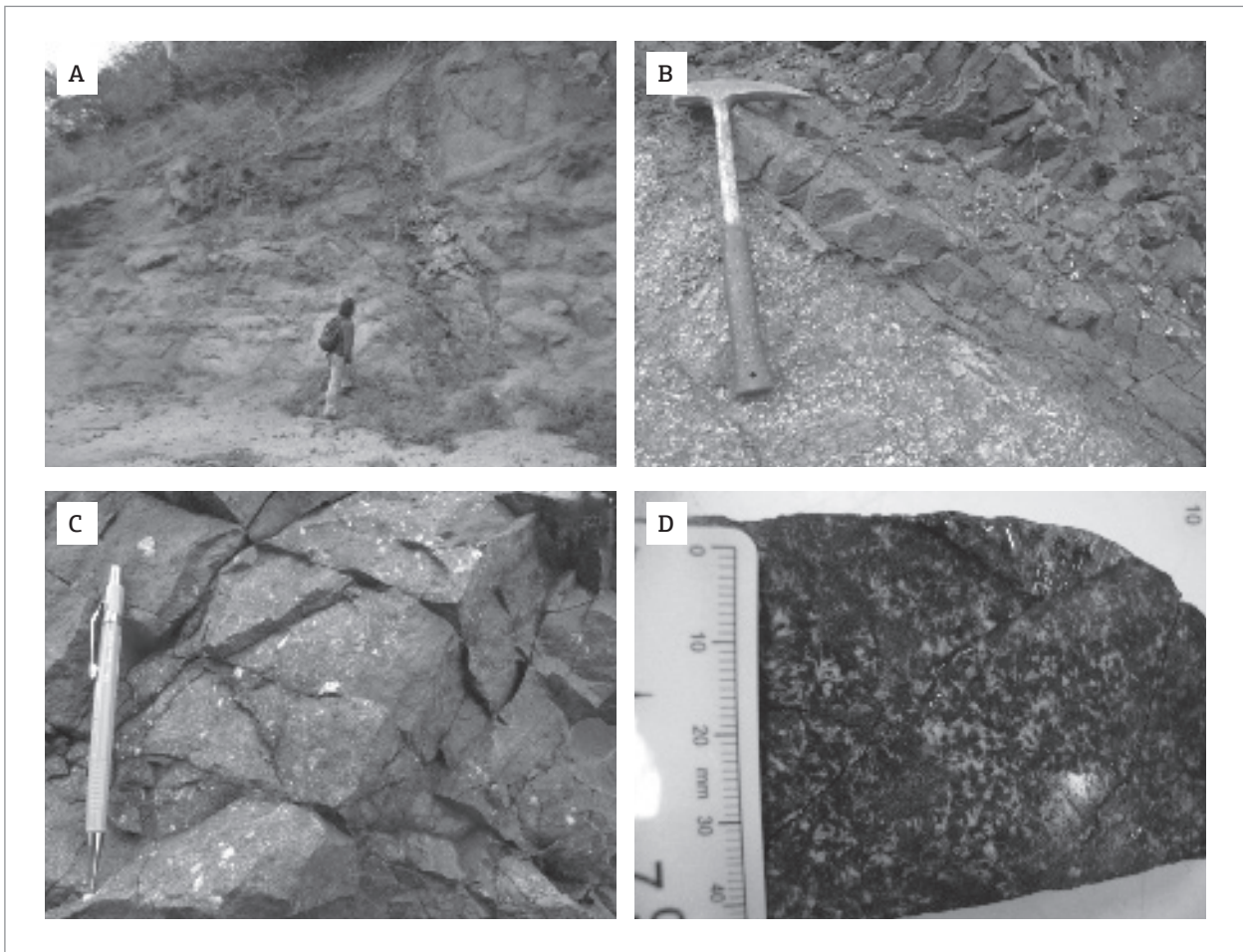


Figure 9. Field and macroscopic aspects of diabase dikes illustrating: (A) and (B) outcrops in abrupt contact with Taquaral Granite; (C) dark-gray, fine-grained rocks in outcrop; (D) Subophitic texture composed of plagioclase laths and mafic minerals.

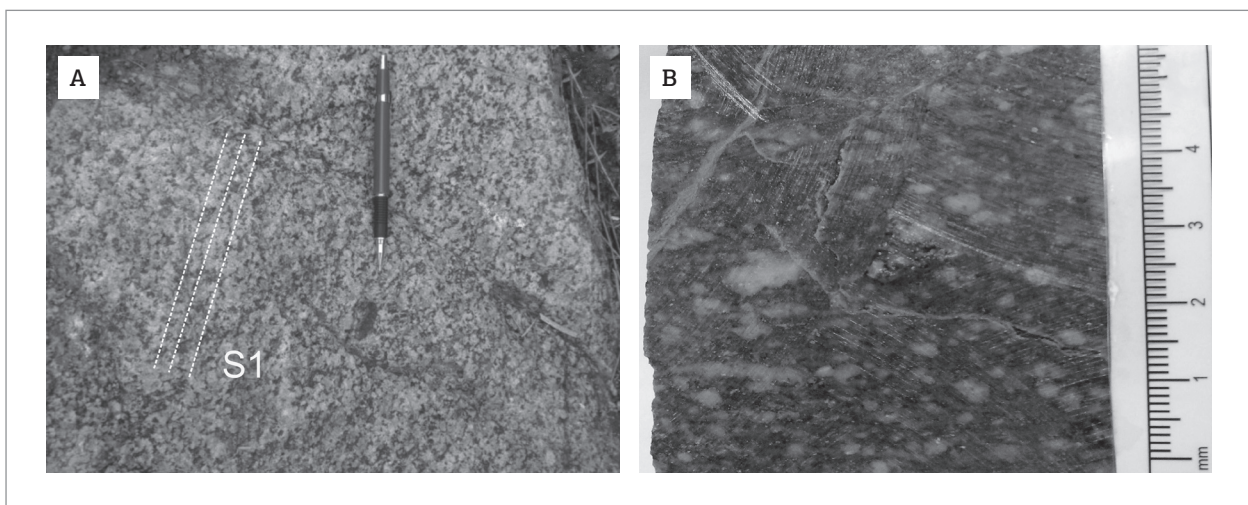


Figure 10. Microphotographs of the Taquaral Granite illustrating F1 deformation products: (A) S_1 foliation in monzogranite showing mafic minerals oriented; (B) mylonite displaying rotated alkali feldspar porphyroclasts in a fine-grained groundmass.

augen texture. Felsic and mafic minerals are preferentially oriented surrounding the porphyroclasts in the groundmass (Fig. 10 B).

S_1 measurements show small variations as illustrated in Fig. 11. S_1 field measurements show a maximum concentration at N10-20 E /80 to 90 NW.

Under the microscope, typical features of ductile deformation are observed, such as quartz ribbons, recrystallized grains of feldspars and quartz (Fig. 12A), kink bands in biotite, deformation twins in plagioclase, and rotated porphyroclasts (Fig. 12B).

The second deformation phase (F_2) is brittle, younger and posterior to the deposition of sedimentary covers

of the Jacadigo and Corumbá Groups. This phase is responsible for the development of fault zones and cataclastic rocks, such as cataclasite, protocataclasite and rarely ultracataclasite.

Two regional faulting systems are identified: one with faults striking N50 to W20 and another with E-W trending faults, both dipping nearly vertically. However, the chronological succession of these structures is not established. The development of thick cataclastic bands is observed in the granitic basement as well as in the sedimentary covers. Cataclasites from the Taquaral Granite and Corumbá Group are products of brittle deformation (F_2) which formed a set of faults nucleating on the central

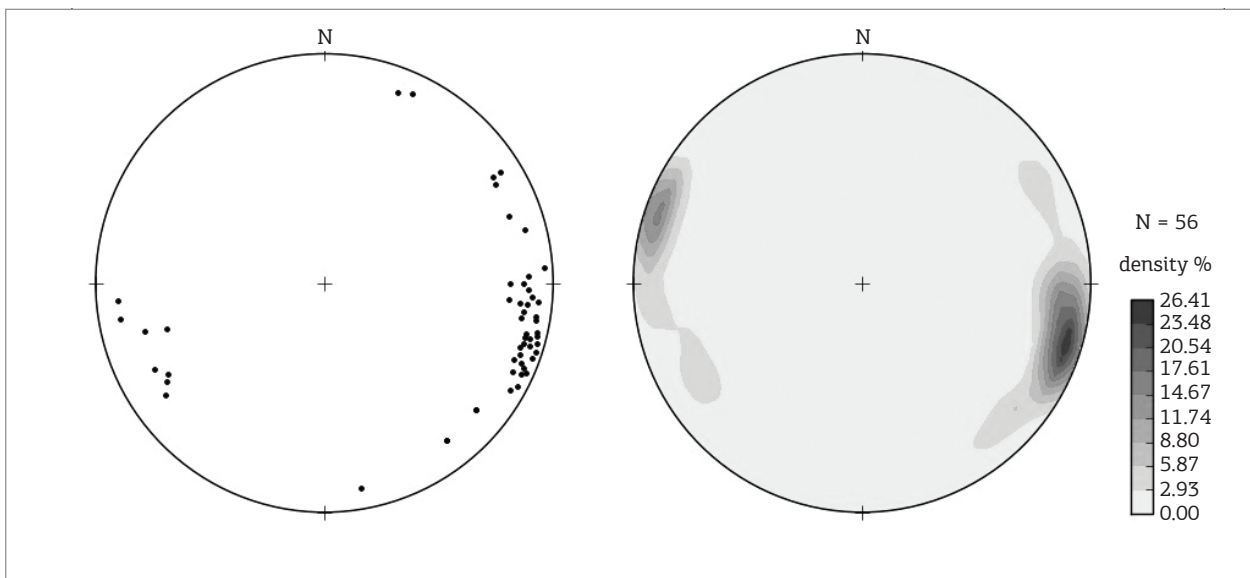


Figure 11. Polar and frequency stereonet of the S_1 foliation of Taquaral Granite showing maximum concentration at 287/82.Lower hemisphere.

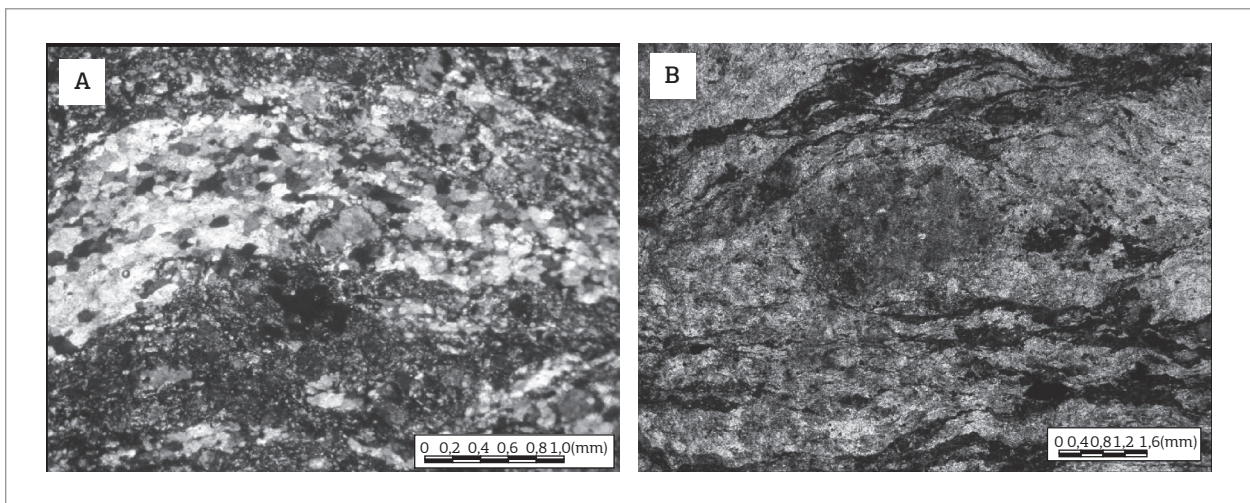


Figure 12. Microphotographs of F_1 illustrating: (A) Level showing sigmoidal aspect consisting of quartz subgrains and recrystallized feldspars; (B) rotated and dusty alkali feldspar porphyroclast. Crossed polarizers in A and parallel in B.

portion and northwest of the study area. The fault rocks are classified as protocataclasites composed of angular to rounded fragments of granite, dolomitic limestone and diabase varying between 1 and 50 cm in a medium to coarse-grained groundmass of granitic composition and carbonate cemented. In general, the contacts between clasts and groundmass are observable (Fig. 13A). The cataclastic bands up to 10 cm thick occur cutting the Taquaral Granite. These bands are composed of angular to rounded grains of quartz, alkali feldspar and plagioclase varying from millimetres to 1-2 cm in a fine-grained groundmass, gray to pink in color. Percolation of hydrothermal fluids occurs parallel to the cataclastic bands leading to silicification, epidotization, chloritization and sericitization (Fig. 13B).

GEOCHEMICAL CHARACTERIZATION

Chemical data of the Taquaral Granite showed wide compositional variation from intermediate to acid rocks with silica content between 60.34 and 75.76% (Tab. 2); GMCF shows values between 60.34 and 61.55%; PCF between 65.47 and 68.64%, and PPF from 75.19 to 75.76 %. Harker diagrams (Fig. 14) indicate negative correlation for the elements TiO_2 , Al_2O_3 , Fe_2O_3 , MgO , CaO and P_2O_5 versus SiO_2 , which may suggest fractional crystallization.

Rocks from the Taquaral Granite are chemically classified as tonalites, granodiorites and syenogranites according to R1-R2 diagram by La Roche (1980; Fig. 15A), and are similarly plotted as quartz monzonites, granites and granodiorite in the Q-P diagram (Debon & Le Fort 1983;

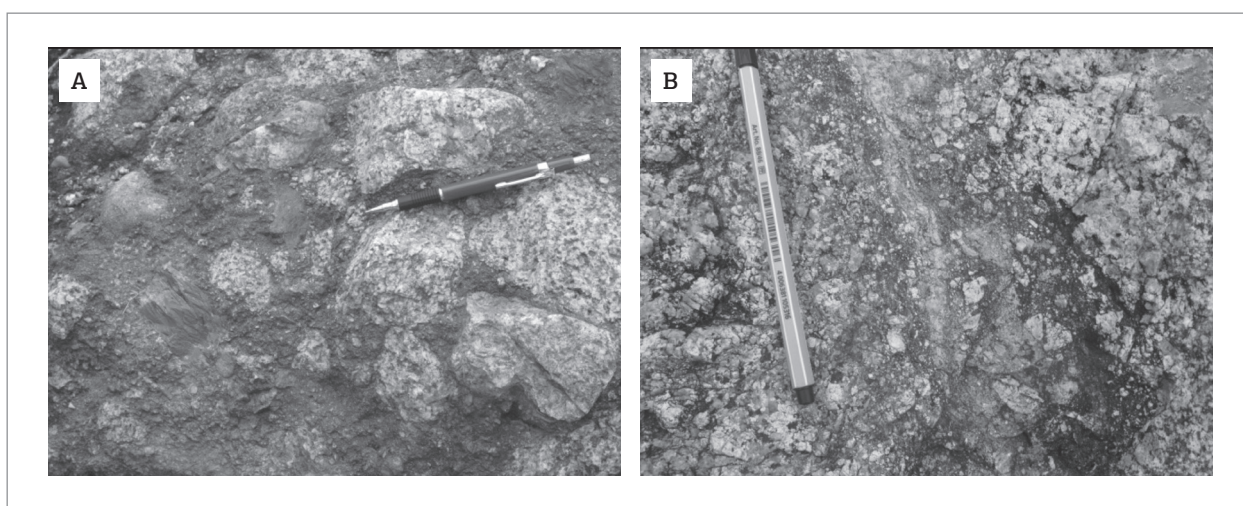


Figure 13. Macroscopic features: (A) protocataclasite composed of angular to rounded fragments of granite, dolomitic limestone and diabase varying from 1 to 50 in diameter in a medium- to coarse-grained groundmass; (B) 10 cm-cataclastic band composed of angular to rounded crystals of alkali feldspar and plagioclase on the scale of millimetres to centimetres set in a finer-grained groundmass, gray to pink in color.

Table 2. Chemical data of the Taquaral Granite (major oxides (weight %), minor and trace elements in weight ppm).

SAMPLE	RM78	RM12	RM92	RM78A	RM11	RM90	RM40	RM09 A	RM92 A
Facies	GMCF ▲	GMCF ▲	GMCF ▲	GMCF ▲	PCF▲	PCF▲	PCF ▲	PPF ●	PPF ●
SiO_2	60.34	61.03	61.36	61.55	65.47	66.75	68.64	75.19	75.76
TiO_2	0.91	0.89	0.95	0.79	0.63	0.60	0.56	0.23	0.16
Al_2O_3	16.17	16.17	15.85	15.92	16.13	14.57	14.99	12.22	12.01
Fe_2O_3	7.66	7.01	7.26	6.81	4.48	4.94	4.14	1.45	1.70
MnO	0.11	0.12	0.13	0.10	0.08	0.08	0.05	0.02	0.03
MgO	2.41	2.15	2.38	2.21	1.69	1.37	1.68	0.10	0.39
CaO	4.81	5.11	4.65	4.83	2.81	2.84	1.76	1.21	1.00
Na_2O_3	3.18	3.08	3.44	3.29	3.60	2.94	3.41	1.81	1.58

Continue...

Table 2. Continuation.

SAMPLE	RM78	RM12	RM92	RM78A	RM11	RM90	RM40	RM09 A	RM92 A
Facies	GMCF ▲	GMCF ▲	GMCF ▲	GMCF ▲	PCF▲	PCF▲	PCF ▲	PPF ●	PPF ●
K ₂ O	2.09	2.37	2.02	2.25	2.94	4.02	2.75	7.05	6.48
P ₂ O ₅	0.32	0.28	0.31	0.29	0.23	0.21	0.18	0.04	0.04
LOI	1.80	1.50	1.40	1.70	1.60	1.30	1.60	0.40	0.50
Total	99.74	99.76	99.77	99.75	99.65	99.66	99.75	99.75	99.63
Ba	807	769	450	712	1840	1857	1332	1458	2715
Be	0.00	2.00	2.00	0.00	3.00	2.00	1.00	0.00	1.00
Co	17.80	15.10	15.90	16.00	7.90	10.10	7.50	1.30	2.80
Cs	1.20	1.40	1.90	1.00	1.10	0.90	1.80	1.10	0.80
Ga	18.50	18.40	19.70	17.70	17.40	15.50	15.20	8.30	8.50
Hf	9.10	6.40	9.50	8.00	5.80	6.20	6.40	5.00	1.40
Nb	8.50	8.50	7.50	6.10	8.00	6.20	8.30	9.80	2.10
Rb	61.30	75.60	76.30	62.50	85.70	99.00	101.10	135.90	97.00
Sr	466.50	414.20	413.30	451.10	423.20	388.90	321.70	246.80	411.50
Ta	0.60	0.60	0.60	0.30	0.60	0.40	0.40	1.10	0.10
Th	5.10	7.30	8.70	6.00	6.90	13.80	9.60	20.80	10.30
U	0.80	1.10	3.40	1.20	1.20	1.60	1.30	1.50	0.60
W	0.70	0.5	0.50	0.90	0.50	0.60	0.50	0.50	0.50
Zr	315.30	269.20	347.80	278.60	208.00	241.10	241.40	165.20	41.80
Y	26.10	29.50	30.00	17.20	27.30	21.40	22.30	33.10	6.90
Pb	5.30	4.70	5.60	5.00	3.40	6.20	3.50	2.50	6.90
La	34.50	37.30	45.90	40.80	43.20	69.50	38.00	78.30	57.90
Ce	77.10	79.10	101.40	78.50	88.20	130.50	78.10	157.90	101.10
Pr	9.30	10.39	12.81	8.71	10.94	14.15	9.66	16.89	9.77
Nd	33.30	42.20	53.80	33.50	46.80	46.00	38.30	61.10	33.00
Sm	5.67	8.65	9.23	4.71	7.94	7.69	6.71	9.87	3.91
Eu	1.36	1.98	2.30	1.56	2.03	1.68	1.69	1.16	0.71
Gd	4.58	7.78	8.07	3.98	6.67	6.12	5.50	7.83	2.97
Tb	0.77	1.09	1.09	0.53	0.88	0.84	0.80	1.17	0.30
Dy	4.41	5.90	5.91	2.62	5.27	4.14	4.43	6.56	1.35
Ho	0.87	1.13	1.04	0.55	1.04	0.86	0.85	1.30	0.31
Er	2.92	2.92	3.35	1.72	2.99	2.25	2.32	3.64	0.66
Tm	0.36	0.45	0.54	0.26	0.37	0.31	0.37	0.50	0.14
Yb	2.66	2.86	3.57	1.59	2.51	1.89	2.19	3.17	0.83
Lu	0.44	0.39	0.46	0.27	0.35	0.29	0.35	0.42	0.11
Eu/Eu*	0.82	0.74	0.81	1.10	0.85	0.75	0.85	0.40	0.64
(La/Yb) _n	8.76	8.81	8.69	17.34	11.63	24.85	11.73	16.69	47.14
(La/Sm) _n	3.74	2.65	3.06	5.33	3.35	5.56	3.48	4.88	9.11
(Gd/Yb) _n	1.37	2.16	1.73	1.99	2.11	2.28	2.00	1.96	2.85

Fig. 15B). Except for a sample plotted as quartz-monzonite, the granodioritic and granitic compositions are supported when using the classification based on normative feldspar in the Ab-An-Or diagram, which is applicable to rocks with normative quartz contents higher than 10% as proposed by O'Connor (1965) and modified by Barker (1979; Fig. 15C).

The $\text{Na}_2\text{O}+\text{K}_2\text{O}-\text{CaO}$ versus SiO_2 diagram by Frost *et al.* (2001; Fig. 16A) assigns to the Taquaral Granite a magnesian subalkaline magmatism, calc-alkaline type, enriched in alkalis. According to the diagram K_2O versus SiO_2 by Peccerillo and Taylor (1976; Fig. 16B), the granite showed medium to high potassium composition.

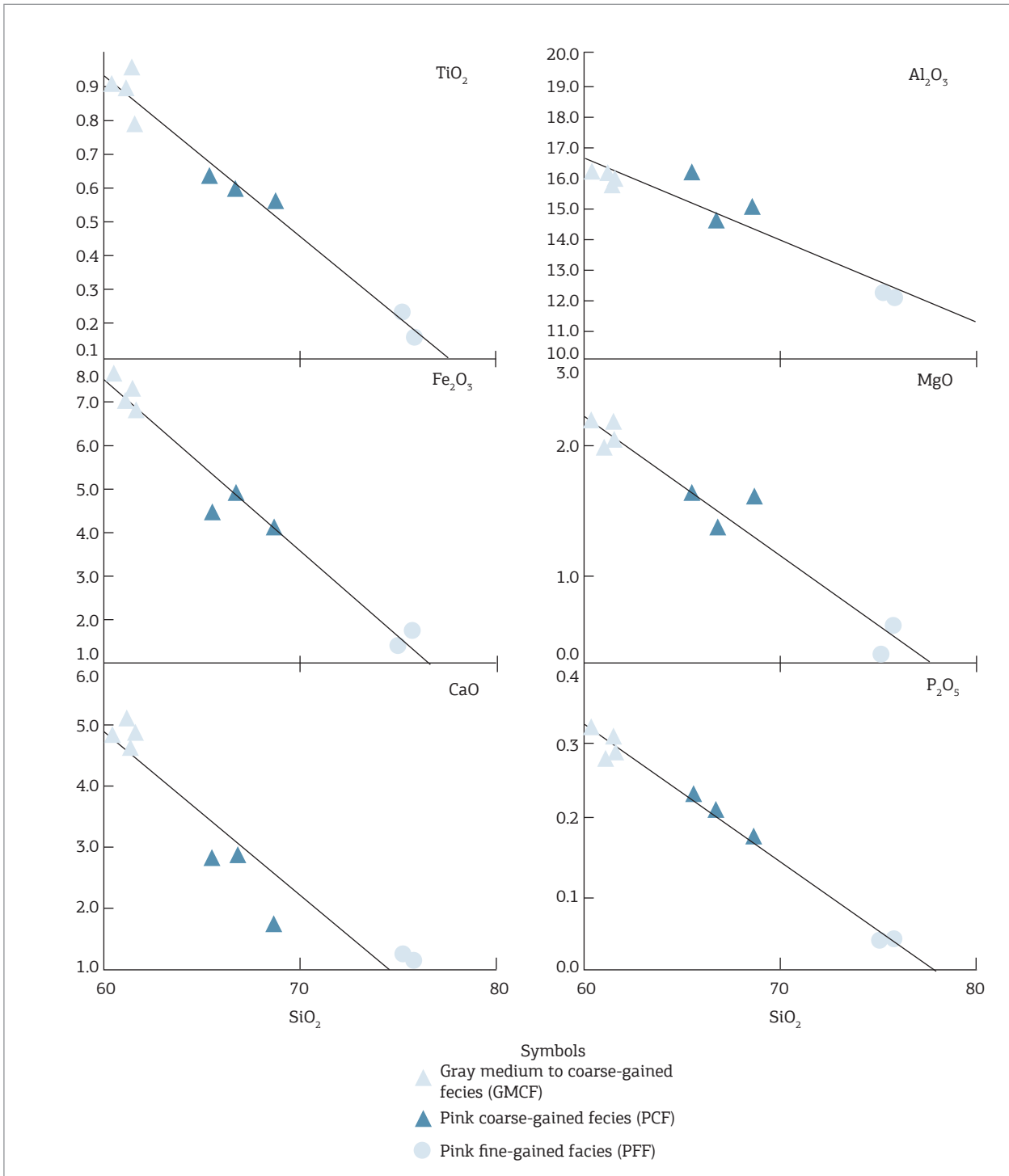


Figure 14. Major-element variation Harker diagrams in weight per cent of oxides for the Taquaral Granite rocks

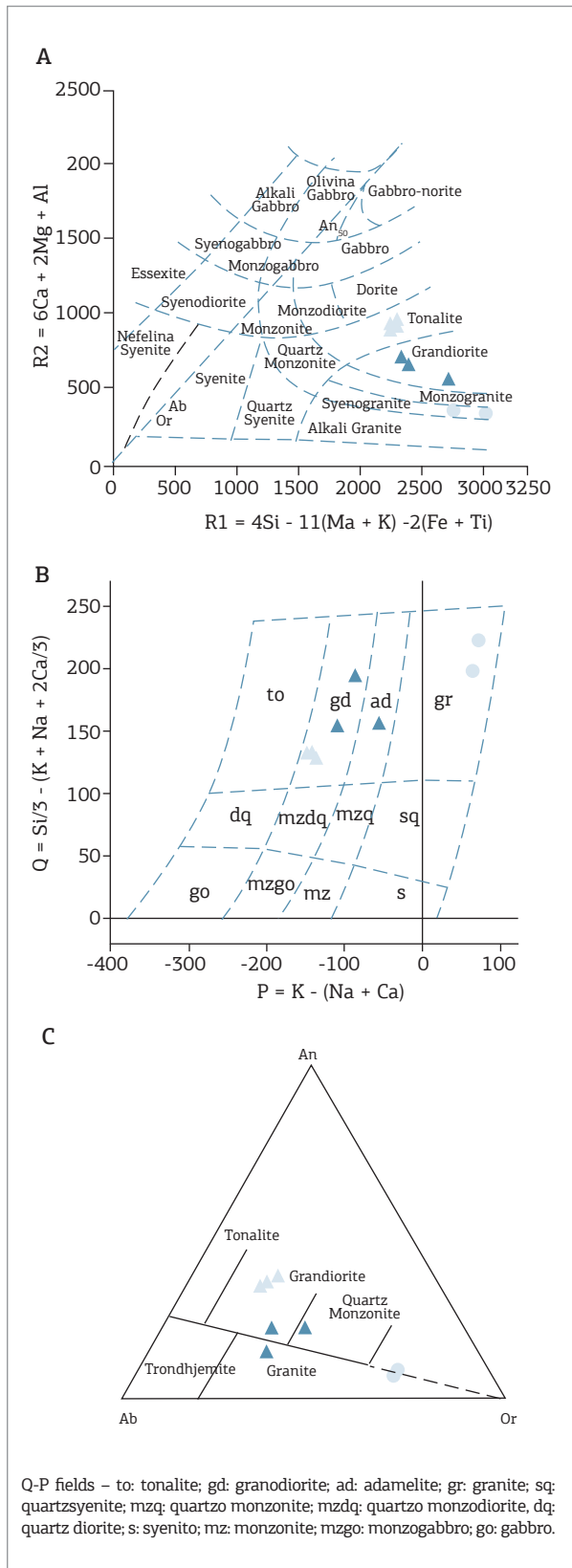


Figure 15. Diagrams showing representative distribution of the Taquaral Granite analyses: (A) R1-R2 (La Roche 1980); (B) Q-P (Debon & Le Fort 1983) fields; (C) Normative An-Ab-Or (O'Connor 1965, modified by Barker 1979).

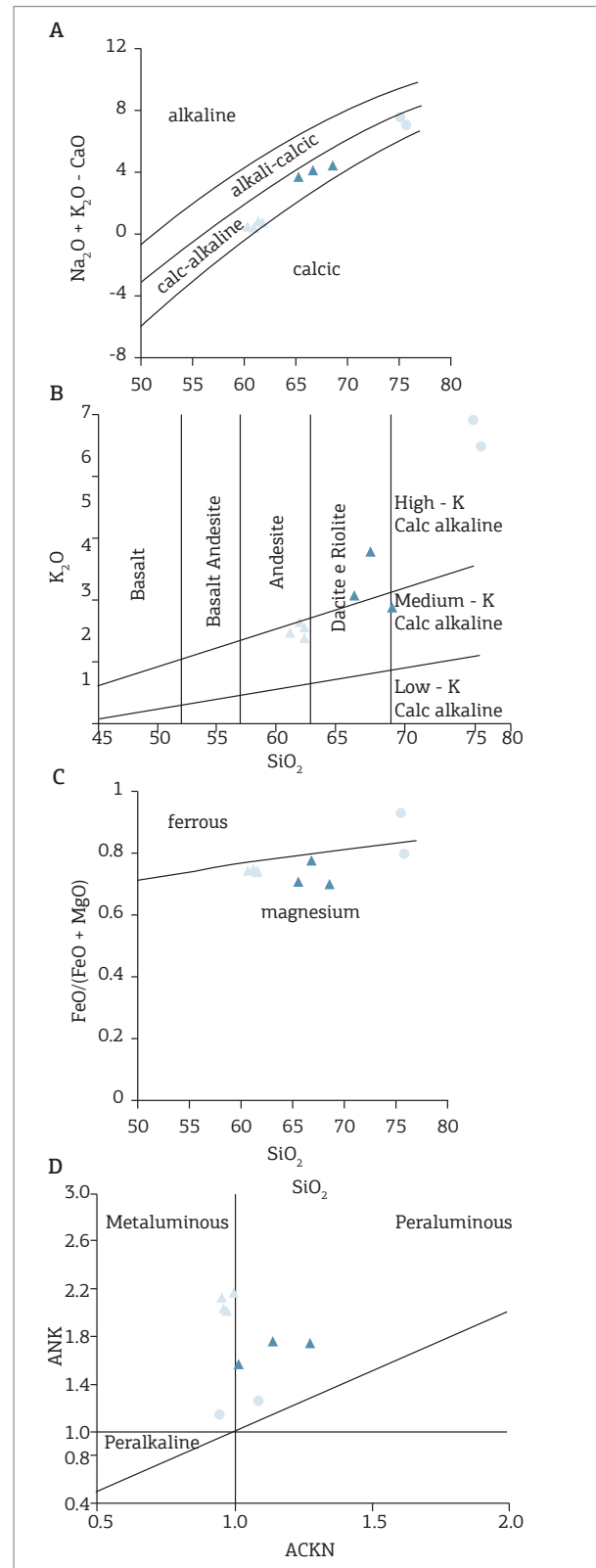


Figure 16. Diagrams showing representative distribution of the Taquaral Granite analyses: (A) Na_2O+K_2O-CaO versus SiO_2 (Frost et al. 2001); (B) K_2O versus SiO_2 (Peccerillo & Taylor 1976); (C) $FeO_{tot}/(FeO_{tot}+MgO)$ versus SiO_2 (Frost et al. 2001) and (D) A/NK versus A/CNK (Maniar & Piccoli 1989).

Excepting one PFF sample, rocks are magnesian granites in the $FeOt/(FeOt+MgO)$ versus SiO_2 diagram (Fig. 16C) proposed by Frost *et al.* (2001). Most of them are classified as metaluminous rocks, however rocks of monzogranitic composition from the GMCF coincide with the peraluminous field in the diagram A/CNK versus A/NK by Maniar & Piccoli (1989; Fig. 16D) which is based on Shand's indexes.

The Taquaral Granite plots representatively within the Magmatic Arc field in the Rb versus $Y+Nb$ (Fig. 17A) and Hf–Rb–Ta (Fig. 17B) diagrams proposed, respectively, by Pearce *et al.* (1984) and Harris *et al.* (1986).

Trace elements pattern associated with K_2O contents, normalized to Ocean Ridge Granites values from Pearce *et al.* (1984; Fig. 18A), shows enrichment in large-ion lithophile elements (LILE) relative to high field strength elements (HFSE) with negative Nb and Ta anomalies, a typical

pattern caused by crustal contribution (Rollinson 1993) or subduction zone settings (Kelemen *et al.* 1993).

The contents of Rare Earth Elements (REE) of the Taquaral Granite show similar pattern to calc-alkaline granitoids with impoverishment of heavy REE relative to light REE when normalized to chondritic values from Sun and MacDonough (1989; Fig. 18B). Heavy REE show subhorizontal pattern with $(Gd/Yb)_N$ ratios between 1.37 and 2.85, and a stronger light REE fractionation expressed by $(La/Sm)_N$ ratio varying from 2.65 to 9.11. An even pattern is observed for the rocks from the GMCF with La/Yb ratios varying from 8.74 to 17.34; PCF samples show La/Yb variation between 11.63 and 28.85 while two PFF samples show distinct La/Yb ratios (16,69 and 47,14). Eu/Eu^* ratio varies between 0.40 and 1.10 for the studied rocks. GMCF samples present this

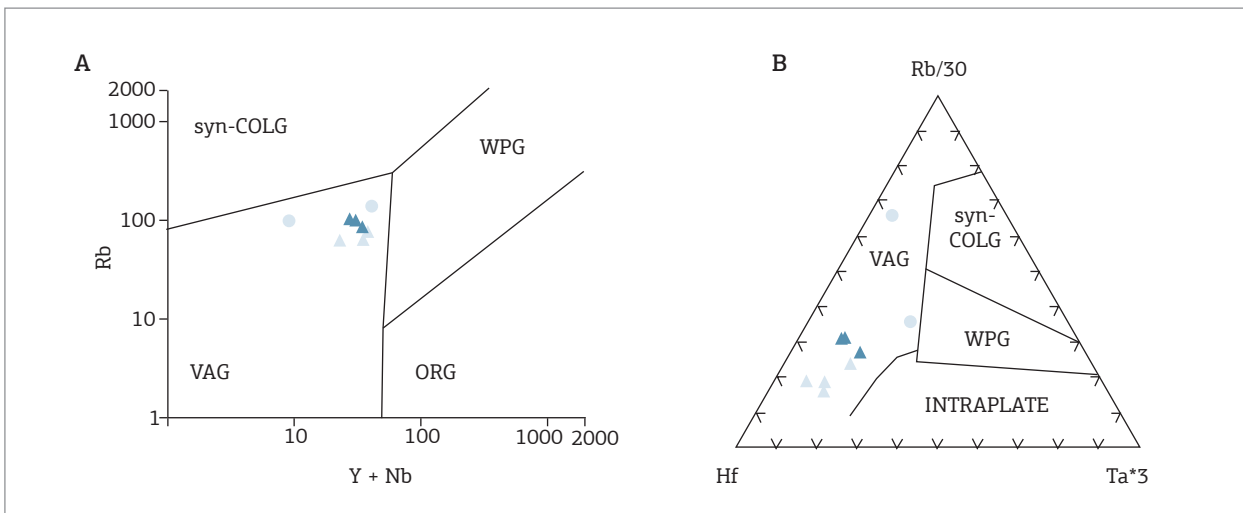


Figure 17. Diagrams showing representative distribution of the Taquaral Granite analyses: (A) Rb versus $Y+Nb$ (Pearce *et al.* 1984); (B) Hf–Rb/30–Ta*3 (Harris *et al.* 1986).

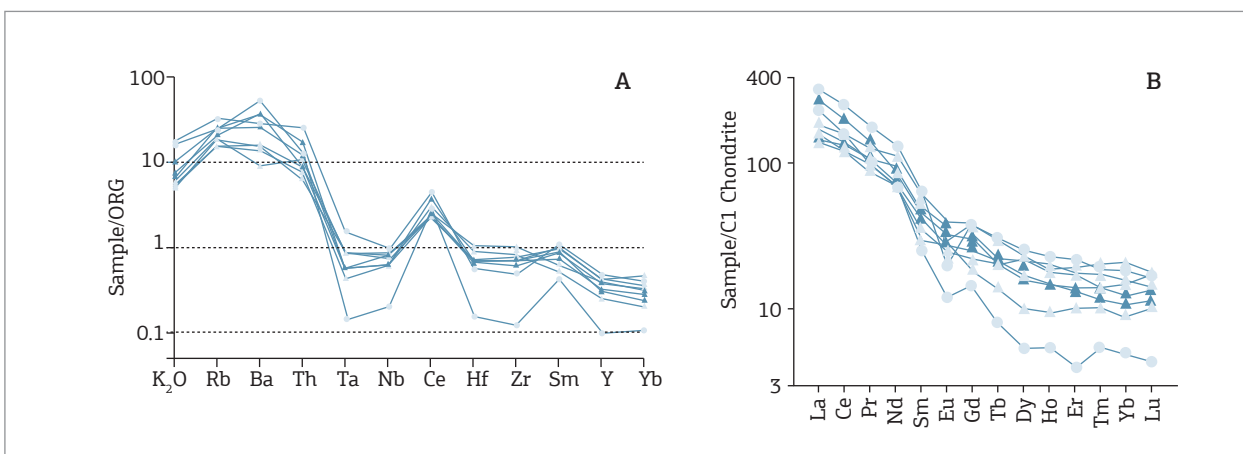


Figure 18. Diagrams showing elemental distribution patterns of the Taquaral Granite: (A) Trace elements and K_2O normalized to Ocean Ridge Granites values according to Pearce *et al.* (1984); (B) REE normalized to C1 chondrite values (Sun & MacDonough 1989).

ratio between 0.74 and 1.10; PCF between 0.75 and 0.85, and PFF between 0.40 and 0.64. One of PFF samples show a strong negative Eu anomaly, however the same pattern for most of them. PFF samples show a vertical displacement due to lower contents of heavy REE indicating greater differentiation.

northeast part of the mapped body. The sample RM-07 (UTM 428893/7891896) was prepared for U-Pb zircon geochronology by SHRIMP and for whole-rock Sm-Nd isotopic analysis together with the sample RM-09A (UTM 429547/7891481). RM-07A belongs to the Gray Medium-to Coarse-grained Facies (GMCF) and RM-09A corresponds to the Pink Fine-grained Facies (PFF).

ISOTOPIC DATA

In order to obtain the crystallization age and characteristics of magmatism, which formed the Taquaral Granite, two samples were collected from the Taquaral Settlement,

U-Pb zircon dating (SHRIMP)

Among the 150 zircon grains handpicked from RM-07, 10 (ten) grains were selected for U-Pb analyses. Most of the selected crystals displays short prism. Some crystals are elongated varying from 80 to 225 μm in length and showing a 3:1 length-width

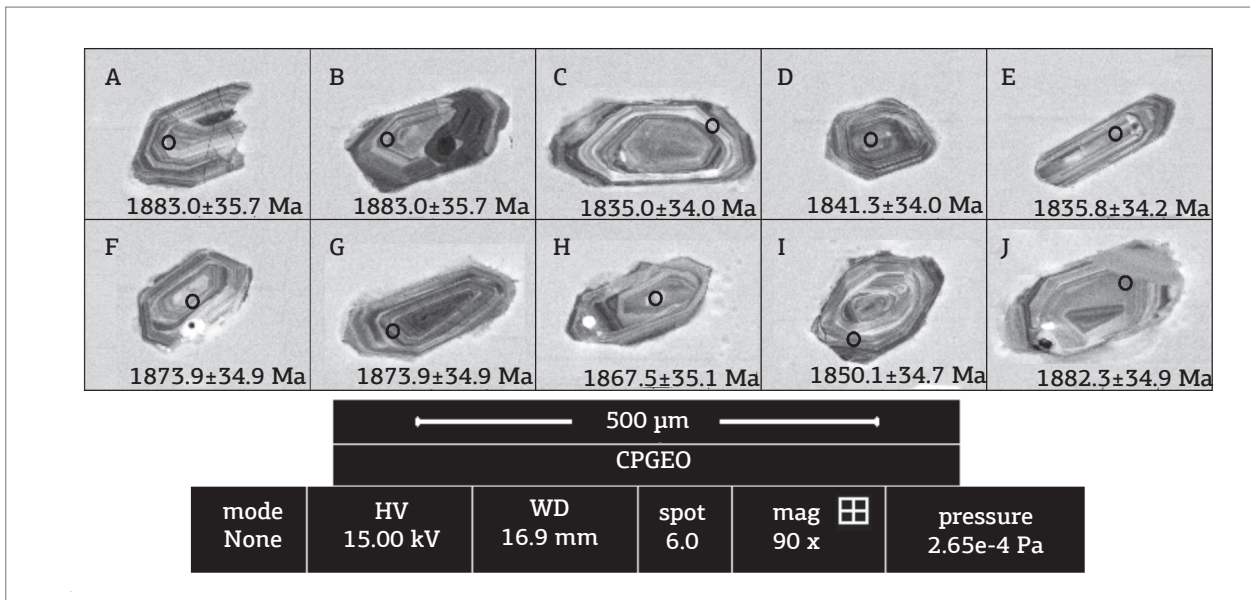


Figure 19. Cathodoluminescence imaging image of zircons from sample RM-07: (A) 2.1; (B) 3.1; (C) 4.1; (D) 5.1; (E) 6.1; (F) 7.1; (G) 9.1; (H) 10.1; (I) 11.1; (J) 12.1. This image also illustrates the zircon pits.

Table 3. SHRIMP U-Pb zircon analyses from sample RM-07.

Grain's symbol	U (ppm)	Th (ppm)	$^{232}\text{Th}/^{238}\text{U}$	$^{206}\text{Pb}/^{238}\text{U}$ %	$^{206}\text{Pb}^*$ (ppm)	$^{207}\text{Pb}/^{235}\text{U}$	\pm %	$^{206}\text{Pb}/^{238}\text{U}$ %	\pm %	$^{207}\text{Pb}/^{206}\text{Pb}$ %	\pm %	$^{206}\text{Pb}/^{238}\text{U}$ Age (Ma)	$\pm 1 \sigma$	$^{207}\text{Pb}/^{206}\text{Pb}$ Age (Ma)	$\pm 1 \sigma$	% disc.	Correted error
2.1	104	92	0.91	0.12	30.4	5.32	2.5	0.3392	2.2	0.1137	1.3	1883.0	35.7	1859.4	23.6	-1	0.858
3.1	138	117	0.88	0.07	39.5	5.24	2.4	0.3338	2.2	0.1139	1.0	1856.7	35.2	1862.3	18.5	0	0.905
4.1	184	153	0.86	0.25	52.2	5.13	2.4	0.3293	2.1	0.1129	1.1	1835.1	34.0	1846.1	20.7	1	0.881
5.1	181	179	1.03	-0.06	51.2	5.31	2.3	0.3306	2.1	0.1165	0.8	1841.3	34.0	1903.0	15.0	3	0.930
6.1	148	180	1.26	0.09	41.8	5.15	2.4	0.3295	2.1	0.1135	1.0	1835.8	34.2	1855.4	17.8	1	0.909
7.1	146	138	0.98	0.00	42.4	5.39	2.3	0.3374	2.1	0.1159	0.9	1873.9	34.9	1893.4	16.9	1	0.916
9.1	398	386	1.00	0.14	112.6	5.11	2.2	0.3289	2.1	0.1126	0.6	1833.0	33.3	1842.5	11.5	1	0.957
10.1	125	114	0.94	0.06	36.2	5.43	2.5	0.3360	2.2	0.1171	1.2	1867.5	35.1	1912.6	20.9	2	0.881
11.1	134	76	0.59	0.07	38.3	5.19	2.4	0.3324	2.2	0.1131	1.0	1850.1	34.7	1850.3	18.7	0	0.902
12.1	155	189	1.25	0.00	45.3	5.26	2.3	0.3391	2.1	0.1124	0.9	1882.3	34.9	1838.7	16.4	-2	0.921

relationship. A few crystals are 1:1. Sometimes they occur fractured or broken, pink in color, varying from nearly incolor to dark.

Cathodoluminescence imaging (CL) of zircons shows relatively regular light and dark band zoning which is interpreted as a variation in U-content as differentiation occurs. The crystal 12.1 shows two growth phases displaying overgrowth rims (Fig. 19J).

The results are shown in Tab. 3. In the U-Pb Concordia diagram (Fig. 20), the zircon analyses furnished a concordant age of 1861 ± 5.3 Ma (1 σ). Taking into consideration the magmatic features of the analysed grains, the age 1861 ± 5.3 Ma is interpreted as the crystallization age of the Taquaral Granite.

Sm-Nd isotopic analyses

Whole rock Sm-Nd analyses from the samples RM-07 and RM-09A show T_{DM} model ages of 2.32 and 2.25 Ga, and strongly negative $\epsilon_{Nd(0)}$ values of -20.05 and -22.98, respectively (Tab. 4). $\epsilon_{Nd(t)}$ values, calculated at a crystallization age of 1861 ± 5.3 Ma, using the U-Pb SHRIMP dating show values of -1.48 for sample RM-07 and -1.28 for sample RM-09A. $\epsilon_{Nd(1,86Ga)}$ negative values and T_{DM} model ages of 2.32 and 2.25 Ga indicate

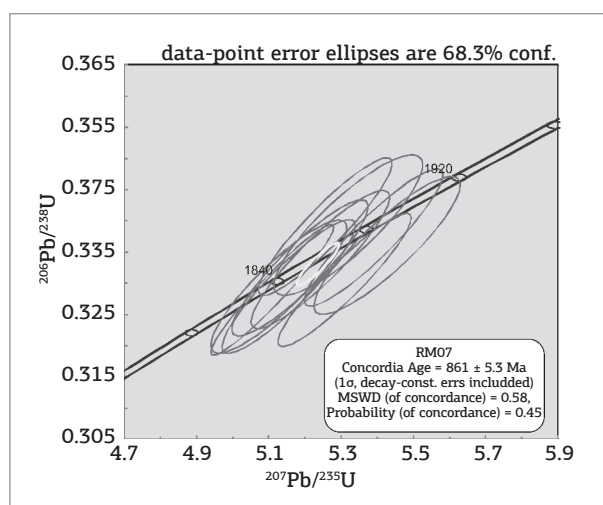


Figure 20. U-Pb Concordia diagram (SHRIMP) of sample RM-07 from the Taquaral Granite showing an upper intercept age at 1861 ± 5.3 Ma which is interpreted as the crystallization age for the granitic body.

a Paleoproterozoic crustal source for both facies of the Taquaral Granite involving partial melting of Rhyacian continental crust.

DISCUSSION AND CONCLUSIONS

The basement underlying the Neoproterozoic sedimentary covers in the region of Corumba has been described by Araújo *et al.* (1982), Del’Arco *et al.* (1982), Godoi *et al.* (2001) and Lacerda Filho *et al.* (2006) as an ensemble of gneisses, amphibolites, metagranites and granodiorites grouped into the Archean Rio Apa Complex. By using field, petrographic and geochronological data it is possible to redefine the basement in this region as a set of Orosirian batholithic granitic intrusions related to the Alumiador Intrusive Suite of Araújo *et al.* (1982).

Studying the Taquaral granite allows recognizing three petrographic facies: Gray Medium- to Coarse-grained Facies (GMCF), Pink Coarse-grained Facies (PCF) and Pink Fine-grained Facies (PFF); as well as two distinct types of enclaves in terms of nature and origin, one of them is an amphibolitic xenolith and the other, a felsic microgranular enclave (FME) having the composition of quartz-diorite. For the latter, an origin related to magma mingling is attributed according to macroscopic features, such as reactive contact with the host rock and engulfment of xenocrystals as well as microscopic features such as poikilitic quartz or corroded quartz, and glomeroporphyros of plagioclase and biotite. Hibbard (1991) suggests that magma mingling is an important process of magmatic differentiation because it results from the interaction between melts of distinct compositions, temperature, density, viscosity and crystallization leading to the formation of hybrid rocks of intermediate composition.

Diabase dikes, which intrude the Taquaral Granite, are representative of an extensional regime. However, the lack of geochronological data is an obstacle in order to establish the igneous event in which these dikes were generated.

Two deformation phases are identified, a ductile phase (F_1) and a brittle phase (F_2). The first deformation phase F_1 developed penetrative foliation and NNE-trending shear zones dipping between 80° and 90° towards the NW. The structural pattern observed for the Taquaral Granite is not

Table 4. Sm-Nd Analytical data of the Taquaral Granite.

Sample	Sm	Nd	$^{147}\text{Sm}/^{144}\text{Nd}$	2σ	$^{143}\text{Nd}/^{144}\text{Nd}$	2σ	f (Sm/Nd)*	$T_{(DM)}$	$\epsilon_{Nd(1.86Ga)}$
RM07 (GMCF)	7.48	37.98	0.11904	0.00022	0.511610	0.000008	-0.395	2.32	-1.48
RM09A (PFF)	13.35	76.16	0.10598	0.00022	0.511460	0.000004	-0.461	2.25	-1.28

similar to the one observed for the Alumiador Intrusive Suite (Rio Apa Terrane) which in turn shows low-dipping foliations, usually lower than 40° towards the SE. Even though structural data from the Correroca Granite are scarce, a similar incipient foliation (Vargas-Mattos 2010) to that of the Taquaral Granite is identified, however there are not enough measurements, making difficult to establish a structural correlation between these units. Kinematic analysis reveals that phase F_1 caused insignificant crustal shortening as a result of a NWW-SEE directed compressive stress leading to tectonic vergence towards the east-southeast. The second phase (F_2) affected both the basement granitic rocks as the rocks from the sedimentary covers represented by the Corumba and Jacadigo Groups causing the nucleation of a set of faults in the Taquaral Granite and Corumba Group and formation of cataclases.

Phases F_1 and F_2 were generated during deformation stages at two different crustal levels. The first phase at crustal levels compatible with the greenschist facies settings and the second phase compatible with shallow crustal settings, likely related to either the evolution of Paraguay Belt and Tucavaca aulacogen or the evolution of Pantanal Basin.

The rocks grouped into the stratigraphic unit called Taquaral Granite are hornblende-biotite granitoids classified as quartz-monzodiorites, quartz-monzonites, granodiorites and monzo to syenogranites. They have intermediate to acidic composition and were generated in magmatic arc settings by a magnesian medium to high K calc-alkaline magmatism, metaluminous to peraluminous.

Isotopic data from the Taquaral Granite indicate a crystallization age of $1,861 \pm 5$ Ma (U-Pb SHRIMP). $\epsilon_{Nd(1,86Ga)}$ values of -1.48 and -1.28 and T_{DM} model ages of 2.32 and 2.25 Ga point out a crustal contribution

to the magma, thus suggesting partial melting of continental crust.

This work dismisses the possibility that Taquaral Granite and Correroca Granite (San Pablo Terrane) are related to the same magmatic event once the latter shows older ages, between 1,925 and 1,894 Ma, and T_{DM} Archean ages between 2.8 and 2.9 Ga differing from the Ryacian model ages for the Taquaral Granite. Similarly, $\epsilon_{Nd(t)}$ values of -8.5 and -9.4 from the Correroca Granite differ significantly from the values obtained for the unit studied here.

Therefore we suggest a correlation between the Taquaral Granite and Alumiador Intrusive Suite (Rio Apa Terrane) once there display petrographic, compositional and age similarities between the Alumiador (Cordani *et al.* 2010), despite their distinct T_{DM} model ages which suggest distinct crustal sources. Regarding the tectonic settings, the Taquaral Granite constitutes an intrusion related to convergent plate boundaries, continental magmatic arc, generated from magma-crust interaction. Considering a correlation between this intrusion and the plutons and batholiths from the Alumiador Intrusive Suite, thus we conclude that the Orosirian Amoguija Magmatic Arc (Lacerda Filho *et al.* 2006) extends to the region of Corumba (MS), in the Brazil-Bolivia frontier.

ACKNOWLEDGMENTS

The authors acknowledge CAPES (PROCAD 096/2007), CNPq (479779/2011-2), Crustal and Tectonic Evolution Research Group “Guaporé” and the GEOCIAM (National Institute of Science and Geosciences Technology of the Amazon) for financial support in research development. The first author is grateful to CAPES for the concession of master’s scholarship and to the Geoscience Postgraduate Program for supporting master studies.

REFERENCES

- Almeida F.F.M. 1967. *Origem e evolução da plataforma brasileira*. Rio de Janeiro, Boletim da Divisão de Geologia e Mineralogia, Boletim 241, p 1-36.
- Alvarenga C.J.S. & Saes G.S. 1992. Estratigrafia e Sedimentologia do Proterozoico Médio e Superior da região Sudeste do Cráton Amazônico. *Revista Brasileira de Geociências*, **22**:493-499.
- Amaral G. 1974. *Geologia Pré Cambriana da Região Amazônica*. Tese de Doutorado, Instituto de Geociências, Universidade de São Paulo, 212 p.
- Araújo H.J.T., Santos Neto A., Trindade C.H., Pinto J.C.A., Montalvão R.M.G., Dourado T.D.C., Palmeira R.C.B., Tassinari C.C.G. 1982. Folha SF. 21 – Campo Grande. In: Brasil. Ministério das Minas e Energia. *Projeto RADAMBRASIL – Geologia*, **28**:23-124.
- Barker O.B. 1979. *A contribution to the geology of the Soutpansberg Group, Waterberg Supergroup, northern Transvaal*. M. Sc. Thesis, Witwatersrand Univ., Johannesburg, 116 p.
- Barreto C.J.S., Lafon J.M., Rosa-Costa L.T., Lima E.F. 2014. Palaeoproterozoic (~1.89 Ga) felsic volcanism of the Iricoumé Group, Guyana Shield, South America: geochemical and Sm-Nd isotopic constraints on sources and tectonic environment. *International Geology Review*, **56**:1332-1356.
- Barros A.M., Silva R.H., Cardoso O.R.F.A., Freire F.A., Souza Jr. J.J., Rivetti M., Luz, D.S., Palmeira R.C., Tassinari C.C.G. 1982. Folha SD. 21, Cuiabá. In: Brasil. Ministério das Minas e Energia. *Projeto RADAMBRASIL – Geologia*, **26**:25-192.
- Bettencourt J.S., Leite Jr W.B., Ruiz A.S., Matos R., Payolla B.L., Tosdal R.M. 2010. The Rondonian-San Ignacio Province in the SW Amazonian Craton: an overview. *Journal of South American Earth Sciences*, **29**:28-46.
- Brites A.F.N., Sousa M.Z.A.M., Ruiz A.S., Batata E.F., Lafon J.M., Plens D.P. 2013. Geologia, petrologia e geocronologia (Pb-Pb) da Formação Serra da Bocaina: evidências de um Arco Magmático Orosiriano no Terreno Rio Apa, sul do Cráton Amazônico. *Brazilian Journal of Geology*, **43**(1):48-69.

- Brito Neves B.B., Sá J.M., Nilson A.A., Botelho N.F. 1995. A Tafrogênese Estateriana nos Blocos Paleoproterozoicos da América do Sul e processos subsequentes. *Geonomos*, **3**:1-21.
- Cordani U.G., Teixeira W., D'Agrella M.S., Trindade R.I. 2009. The position of the Amazonian Craton in supercontinents. *Gondwana Research*, **15**:396-407.
- Cordani U.G., Teixeira W., Tassinari, C.C.G., Ruiz A.S. 2010. The Rio Apa Craton in Mato Grosso do Sul (Brazil) and Northern Paraguay: geochronological evolution, correlations and tectonic implications for Rodinia and Gondwana. *American Journal of Science*, **310**:1-43.
- Correia Filho F.C.L., Martins E.G., Araújo E.S. 1981. *Projeto Rio Apa: Relatório da área I*. Goiânia: CPRM, Convênio CODESUL/CPRM, v. 2.
- Debon F. & Le Fort P. 1983. A chemical mineralogical classification of common plutonic rocks and associations. *Trans. R. Soc. Edinburgh: Earth Science*, **73**:135-149.
- Del'Arco J.O., Silva R.H., Tarapanoff I., Freire F.A., Pereira L.G.M., Souza S.L., Luz J.S., Palmeira R.C.B., Tassinari, C.C.G. 1982. Geologia. In: Brasil. Ministério das Minas e Energia, Projeto RADAMBRASIL, Folha SE.21. Corumbá e Parte da Folha SE 20. Geologia, **27**:25-160.
- De Paolo D.J. 1981. Trace elements and isotopic effects of combined wallrock assimilation and fractional crystallization. *Earth and Planetary Science Letters*, **53**:189-202.
- Frost B.R., Barnes C.G., Collins W.J., Arculus R.J., Elis D.J., Frost C.D. 2001. A Geochemical Classification for Granitic Rocks, *Journal of Petrology*, **42**:2033-2048.
- Godoi H.O., Martins E.G., Mello J.C.R., Scislewski G. 2001. Programa de Levantamentos Geológicos Básicos do Brasil - PLGB: folha SE.21-Y-D - Corumbá; Folha SF.21-V-B- Aldeia Tomázia; Folha SF.21-V-D - Porto Murtinho: escala 1:250 000. Brasília, CPRM, 88 p.
- Godoy A.M., Manzano J.C., Araújo L.M.B., Silva J.A. 2010. Suíte Vulcânica Serra da Bocaina, Grupo Amoguijá - Maciço Rio Apa - MS. São Paulo, UNESP, *Geociências*, **29**:571-587.
- Grohmann C.H., Campanha G.A.C., Soares Junior A.V. 2011. OpenStereo: um programa livre e multiplataforma para análise de dados estruturais. In: Simpósio Nacional de Estudos Tectônicos, 13. Atas, p. 26-28.
- Harris N.B.W., Pearce J.A., Tindle A.G. 1986. *Geochemical characteristics of collision-zone magmatism*. In: Coward M.P. & Ries, A.C. (eds) *Special Publications of Geological Society*, London, **19**:67-81.
- Hibbard M.J. 1991. Textural anatomy of twelve magma-mixed granitoid systems. In: Didier J. & Barbarin B. (Eds.) *Enclaves and granite petrology*. Amsterdam: Elsevier., p: 431-444.
- Hutchinson C.S. 1974. *Laboratory handbook of petrographic techniques*. New York: John Wiley & Sons. 527 p.
- Kelemen P.B., Shimizu N., Dunn T. 1993. Relative depletion of niobium in some arc magmas and the continental crust: partitioning of K, Nb, La and Ce during melt/rock reaction in the upper mantle. *Earth Planet. Sci. Lett.*, **120**:111-134.
- Lacerda Filho J.W., Brito R.S.C., Silva M.G., Oliveira C.C. De, Moreton L.C., Martins E.G., Lopes R.C., Lima T.M., Larizzatti J.H., Valente C.R. 2006. *Geologia e Recursos Minerais do Estado de Mato Grosso do Sul*. Programa integração, atualização e difusão de dados de geologia do Brasil. Convênio CPRM/SICME - MS, MME, 10. 28 p.
- La Roche H. 1980. Granites chemistry through multicationic diagrams. *Sciences de la Terre, Série Informatique Géologique*, **13**:65-88
- Le Maitre R.W. 2002. *Igneous rocks: a classification and glossary of terms: recommendations of the international union of geological sciences subcommission on the systematics of igneous rocks*. Cambridge, Cambridge University Press, 236 p.
- Litherland M. & Klinck B.A. 1982. Introducing the terms: "Paraguá Cráton" and "Pensamiento Granitoid Complex" for use in sheet reports. *Rep East Bolivia Miner Expl Proj.*, Santa Cruz, ML/37 (Unpublished).
- Litherland M., Annells R.N., Appleton J.D., Berrangé J.P., Bloomfield K., Burton C.C.J., Darbyshire D.P.F., Fletcher C.J.N., Hawkins M.P., Klinck B.A., Lanos A., Mithcell W.I., O Connor E.A., Pitfield P.E.J., Power G.E., Webb B.C. 1986. *The Geology and Mineral Resources of the Bolivian Precambrian Shield*. British Geological Survey. Overseas Memoir 9. London: Her Majesty's Stationery Office. 140 p.
- Ludwig K.R. 2001. User's manual for Isoplot/Ex. rev. 2.49. A Geochronological Toolkit for Microsoft Excel. Berkeley Geochronological Center. 45 p. (Special Publication 1A)
- Lugmair G.W. & Marti K. (1978). Lunar initial ¹⁴³Nd/¹⁴⁴Nd: differential evolution of the lunar crust and mantle. *Earth and Planetary Science Letters*, **39**:349-357.
- Maniar P. D. & Piccoli P.M. 1989. Tectonic discrimination of granitoids. *Geological Society American Bulletin*, **101**:635-643.
- Manzano J.C., Godoy A.M., Araújo L.M.B., Godoy L.P. 2012. Suíte Plutônica Alumizador, Grupo Amoguijá, Maciço Rio Apa - MS. São Paulo, UNESP, *Geociências*, **31**(3):351-370.
- Nogueira S. F., Sousa M. Z. A., Ruiz A. S., Batata M. E. F., Cabrera R. F., Costa J. T. 2013. Granito Aquidabã - Suíte Intrusiva Alumizador - Sul do Cráton Amazônico - Geologia, Petrografia e Geoquímica. In: Anais do Simpósio de Geologia da Amazônia, Belém, 13º, SBG-NO, Belém, p. 368-371.
- O'Connor J.T. 1965. A classification for quartz-rich igneous rocks based on feldspar ratios. *US Geological Survey*, 525B, 79-84.
- Oliveira E.C., Lafon J.M., Gioia S.M.C.L., Pimentel M.M. 2008. Datação Sm-Nd em rocha total e granada do metamorfismo granulítico da região de Tartarugal Grande, Amapá Central. *Revista Brasileira de Geociências*, **38** (1): 114-127.
- Passchier C.W. & Trouw R.A.J. 2005. *Microtectonics*, 2nd ed., Germany, Springer-Verlag, 366 p.
- Peccherillo R. & Taylor S. R. 1976. Geochemistry of Eocene calc-alkaline volcanic rocks from the Kastamonu area, northern Turkey. *Contributions to Mineralogy and Petrology*, **58**: 63-81.
- Pearce J.A., Harris N.B.W., Tindle A.G. 1984. Trace element discrimination diagrams for the tectonic interpretation of granitic rocks. *Journal of Petrology*, **25**(4):956-983.
- Plens D.P., Ruiz A.S., Sousa M.Z.A.M., Batata E.F., Lafon J.M., Brittes A.F.N. 2013. Batólito Cerro Porã: granito tipo-A pós-orogênico do arco magmático Amoguijá - Terreno Rio Apa - sul do Cráton Amazônico. *Brazilian Journal of Geology*, **43**(3):515-534.
- Rollinson H.R. 1993. *Using geochemical data: evaluation, presentation, interpretation*. Longman Geochemistry Series.
- Ruiz A.S. 2005. *Evolução geológica do sudoeste do Cráton Amazônico região limítrofe Brasil-Bolívia - Mato Grosso*. Tese de Doutorado, Instituto de Geociências e Ciências Exatas, Universidade Estadual Paulista, 14-245 p.
- Ruiz A.S., Simões L.S.A., Almeida H.L., Godoy A.M., Manzano J.F. 2005. Análise estrutural do batólito Santa Helena: implicações sobre a evolução tectônica do SW do Cráton Amazônico durante as Orogenias San-Ignácio-Rondoniano e Sunsás-Aguapeí. In: X Simpósio de Estudos Tectônicos, Curitiba, Anais, p. 411-414.
- Ruiz A.S., D'Agrella Filho M.S., Sousa M.Z.A., Lima G.A. 2010. Tonian sills and mafic dike swarms of S-SW Amazonian Craton: records of Rodinia Supercontinent breakup? In: The Meeting Of The Americas. Foz do Iguaçu. Abstracts Foz do Iguaçu: The Meeting of the Americas, 2010, v. único.

- Sá E.F.J. & Hackspacher P.C. 1982. Revisão sobre análise estrutural, parte 1 - conceituação básica e métodos. *Ciências da Terra*, **5**:24-36.
- Saes G.S. & Leite J.A.D. 1993. Evolução tectono-sedimentar do Grupo Aguapeí, Proterozoico Médio na porção meridional do Cráton Amazônico: Mato Grosso e Oriente Boliviano. *Revista Brasileira de Geociência*, **23**(1):31-37.
- Saes G.S. & Fragoso César A.R.S. 1994. The Aguapeí basin (Southwest Amazonia): A Grenville age aulacogen of the Sunsás orogeny. In: SBG, 38° Congresso Brasileiro de Geologia. Atas 1, 207-209.
- Saes G.S. & Fragoso César A.R.S. 1996. Acreção de terrenos mesoproterozoicos no SW da Amazônia. In: SBG, Congresso Brasileiro de Geologia, 39, Atas, p. 348.
- Saes G.S. 1999. *Evolução Tectônica e Paleogeográfica do Aulacógeno Aguapeí (1.2-1.0 Ga) e dos Terrenos do seu Embasamento na Porção sul do Cráton Amazônico*. Tese de Doutorado, Instituto de Geociências, Universidade de São Paulo, 135 p.
- Santos J.O.S., Hartmann L.A., Gaudette H.E., Groves D.I., McNaughton N.J., Fletcher I.R. 2000. A new understanding of the Amazon Craton Provinces based on integration of field mapping and U-Pb and Sm-Nd Geochronology. *Gondwana Research*, **3**:453-488.
- Santos J.O.S., Rizzotto G.J., Potter P.E., McNaughton N.J., Matos R.S., Hartmann L.A., Chemale Jr. F., Quadros M.E.S. 2008. Age and autochthonous evolution of the Sunsás Orogen in West Amazon Craton based on mapping and U Pb geochronology. *Precambrian Research*, **165**:120-152.
- Sato K., Basei M.A.S., Siga O.J., 2008. Novas técnicas aplicadas ao método U-Pb no CPGeo - IGC/USP: avanços na digestão química, espectrometria de massa (TIMS) e exemplos de aplicação integrada com SHRIMP. In: *Geol. USP Série Científica*, **8**:77-99.
- Sibson R.H. 1977. Fault rocks and fault mechanisms. *Journal of the Geological Society*, **133**:191-213.
- Stern R.A. 1998. High-resolution SIMS determination of radiogenic trace-isotopic ratios in minerals. In: Cabri, L.J., Vaughan, D.J (Eds). *Modern approaches to ore and environmental mineralogy*. Mineralogical association of Canada. Short Course Series, **27**:241-268.
- Streckeisen A.L. 1976. To each plutonic rock its proper name. *Earth Science Review*, **12**:1-35.
- Sun S.S. & MacDonough W.F. 1989. Chemical and isotopic systematics of oceanic basalts: implications for mantle composition and process. *Geological Society London*, **1**:1313-345.
- Tassinari C.C.G. & Macambira, M.J.B. 1999. Geochronological provinces of the Amazonian Craton. *Episodes*, **38**:174-182.
- Tassinari C.G.C. & Macambira M.J.B. 2004. A Evolução Tectônica do Cráton Amazônico. In: Neto-Mantesso V., Bartorelli A, Carneiro C. D. R., Brito-Neves, B.B. (eds). *Geologia do Continente Sul-Americano: Evolução da Obra de Fernando Flávio Marques de Almeida*, p. 471-486.
- Teixeira W., Geraldés M.C., Matos R., Ruiz A.S., Saes G., Vargas Mattos G. 2010. A review of the tectonic evolution of the sunsás belt. SW Amazonian Craton. *Journal of South American Earth Sciences*, **29**:47-60.
- Trompette R., Alvarenga C.J.S., Walde D. Geological evolution of the Neoproterozoic Corumbá graben system (Brazil). 1998. Depositional context of the stratified Fe and Mn ores of the Jacadigo Group. *Journal of South American Earth Sciences*, **11**:587-597.
- Vargas-Mattos G.L. 2010. *Caracterização geocronológica e geoquímica dos granitos proterozoicos: implicação para a evolução crustal da borda SW do Cráton Amazônico na Bolívia*. Tese de Doutorado, Faculdade de Geologia, Universidade do Estado do Rio de Janeiro, 164 p.
- Williams I. 1998. U-Th-Pb geochronology by ion microprobe, In: McKibben M.A., Shanks III W.C., Ridley W.I., (eds), Applications of microanalytical techniques to understanding mineralizing processes. *Reviews in Economic Geology*, **7**:1-35.

Arquivo digital disponível on-line no site www.sbgeo.org.br
